

ASSESSMENT OF GNSS COMPUTED ZHD AND ZWD FOR POINTS OF DIFFERENT ELEVATION

MASATU JOHN MASATU

A dissertation submitted to the Department of Geospatial Science and Technology in partial fulfilment of the requirement for the award of Bachelor of science degree in Geomatics of Ardhi University on June 2023.

CERTIFICATION

The undersigned certify that they have proof read and hereby recommend for acceptance of a dissertation titled “**Assessment of GNSS Computed ZWD And ZHD For Points of Different Elevation**” in partial fulfilment of the requirements for the award of degree of Bachelor of Science in Geomatics at Ardhi University, Dar es salaam.

.....

Dr. Elifuraha Saria

(Main Supervisor)

Date

DECLARATION AND COPYRIGHT

I Masatu Masatu J hereby declare that, the content of this dissertation are the result of my own findings through my study and investigation, and to the best of my knowledge they have not been presented anywhere else as a dissertation for diploma, degree or any similar academic award in any institution of higher learning.

.....

Masatu, Masatu J

22803/T.2019

(Candidate)

Copyright ©1999 This dissertation is copyright material protected under the Berne Convention, the Copyright Act of 1999 and other international and national enactments, in that behalf, on intellectual property. It may not be reproduced by any means, in full or in part, except for short extracts in fair dealing; for research or for private study, critical scholarly review or discourse with an acknowledgement, without the written permission of the Directorate of Undergraduate studies, on behalf of both the author and Ardhi University.

ACKNOWLEDGMENT

First and foremost, I would like to begin by expressing my utmost gratitude to the Lord, the Almighty, for guiding and supporting me throughout my journey and for bringing me this far. I firmly believe that His presence and guidance have been instrumental in my achievements, and I trust that He will continue to be by my side in all future endeavours.

I would like to extend my heartfelt appreciation to my supervisor, Dr. Elifuraha Saria, for his guidance, support, and invaluable insights throughout the entire research process. His expertise and encouragement have been pivotal in shaping the direction of this study and ensuring its successful execution. I am truly grateful for his mentorship and the knowledge I have gained under his guidance.

I would also like to express my sincere thanks to Mr. Timoth Joseph, Mr Daudi Ntambila and Ms. Valeria Ayubu, as well as the entire academic staff of the Department of Geospatial Sciences and Technology (DGST) at Ardhi University. Their guidance and expertise have played a significant role in shaping my academic and research journey. I am grateful for their dedication to teaching and for creating a nurturing learning environment.

I would also like to happily thank my lovely family; my parents Mr & Mrs John Masatu, my sisters Perus and Nancy John Masatu May God protect you, always

Furthermore, I would like to acknowledge and extend my gratitude to my fellow colleagues Johnson Kiluswa, Daniel Sospeter, Salma Kodi, Abdalah Machemba, Jumanne Masembo, Benedict Mramba, Charles Urrio, and all my Geomatics and Geoinformatics classmates for their unwavering support and companionship throughout this achievement.

In conclusion, I am deeply grateful to all those who have contributed to my academic and research journey. My appreciation extends to my supervisor, the academic staff, my fellow colleagues, and my dear friends. Each one of you has played a unique role in my success, and I am truly blessed to have had your support. May God bless each and every one of you abundantly.

DEDICATION

This research is wholeheartedly dedicated to my beloved parents, who have been a source of inspiration and gave me strength, who continually provide their moral, spiritual, emotional and financial support. To my sisters, brothers, relatives, mentor, friends who shared their words of advice and encouragement to finish this study at a time.

Lastly, I dedicated this book to the almighty god, thank you for the guidance, strength, power of mind and skills for giving us a healthy life.

ABSTRACT

Tropospheric error is a primary error source in the earth observation and variety of radio navigation. The accurate estimation of Zenith Hydrostatic Delay (ZHD) and Zenith Wet Delay (ZWD) is essential for precise Global Navigation Satellite System (GNSS) positioning and meteorological and geodetic application. The ZHD and ZWD parameters play a crucial role in meteorological and geodetic applications, such as precise positioning, atmospheric correction, and weather forecasting. Elevation is a fundamental geographical parameter that plays a crucial role in various meteorological and geodetic applications. It refers to the height or altitude of a specific point above sea level and is a key factor in understanding the Earth's atmospheric conditions and weather patterns. In this study the relationship between ZTD and elevation and location of station is analysed. It presents an assessment of GNSS computed ZHD and ZWD values for points of different elevation. The objective is to assess the impact of elevation on the accuracy of ZHD, ZWD and ZTD estimations for points of different stations. In this research the GNSS data were processed using GAMIT/GLOBK. Where by Data processing involves process phase data for one year from Jan 2015 to Dec 2015 to produce daily loose solution and o files and h file for each day. This was then input into metutil script. The results were ZHD, ZWD and their uncertainties. Using the relationship of ZWD and ZHD other parameters were determined. The results and analysis done reveal that ZHD varies due to tropospheric thickness variation in different elevation but also differences in surface pressure. ZWD it varies due to variation of atmospheric moisture delays, as higher elevation points experience lower atmospheric moisture content, resulting in reduced delays caused by water vapour. And ZTD values decreases as height increases imply that points at higher elevations experience less atmospheric delay in GNSS signal propagation. For example, ARSH (1345.161m) have more less delay of 2144.46mm compared to the other low elevation point MTVE (-11.414m) which have large delay of 2615.67mm the variation of atmospheric temperature and pressure with height which contributed to delay of GNSS signals from the satellite to receiver. Investigation can be done on long-term trends, studying different geographical regions, and considering the influence of local weather patterns that can provide deeper insights into the elevation-dependent behaviour of ZTD.

Keywords: Zenith Tropospheric Delay (ZTD), Zenith Hydrostatic Delay (ZHD), Zenith Wet Delay (ZWD).

TABLE OF CONTENTS

CERTIFICATION	i
DECLARATION AND COPYRIGHT.....	iii
ACKNOWLEDGMENT.....	iv
DEDICATION	v
ABSTRACT.....	vi
TABLE OF CONTENTS.....	viii
LIST OF FIGURES	xi
LIST OF TABLES	xii
ACRONYMS AND ABBREVIATIONS	xiii
CHAPTER ONE	1
INTRODUCTION.....	1
1.0.1 Zenith dry or hydrostatic delay (ZHD).....	2
1.0.2 Zenith wet delay (ZWD).....	2
1.1 Statement of the problem	4
1.2 Main objective.....	5
1.3 Specific objectives.....	5
1.4 CORS locations used in this study	5
1.5 Significance of the research	6
1.6 Scope and limitation.....	7
1.7 Organization of the study	7
CHAPTER TWO	8
LITERATURE REVIEW.....	8
2.1 Global Navigation Satellite System	8
2.1.1 Main principle of GNSS	8

2.1.2 GNSS segments	9
2.1.3 GNSS Signal and Observables	10
2.1.3 GNSS applications.....	12
2.1.4 GNSS positioning techniques.....	13
2.2 GNSS Error Sources.....	14
2.2.1 Tropospheric errors.....	14
2.3 Mapping Functions.....	20
2.3.1 ZWD from total zenith tropospheric delay	21
2.4 Related studies.....	23
CHAPTER THREE	25
METHODOLOGY	25
3.1 Data Source and Acquisition.....	25
3.1.1 RINEX observation, meteorological, navigation files for experiment sites and RINEX observation files for IGS sites.	25
3.1.2 Precise ephemeris and precise clock files.....	27
3.2 Data preparation	28
3.2.1 RINEX observation files for experiment and IGS sites.	28
3.2.2 RINEX navigation files	28
3.3 RINEX meteorological file	29
3.4 Data processing	29
3.4.1 Data processing by gamit	29
CHAPTER FOUR.....	35
RESULTS AND ANALYSIS	35
4.1 3D positioning.....	35
4.2 Zenith Hydrostatic Delay ZHD	36

4.2.1 Graph of ZHD against elevation.....	36
4.3 Zenith Wet Delay	38
4.3.1 Graphs of ZWD	39
4.4 Zenith Total Delay	41
4.4.1 Graph of ZTD	42
CHAPTER FIVE	45
CONCLUSION AND RECOMMENDATION	45
5.1 Conclusion.....	45
5.2 Recommendation.....	46
REFERENCES	47
APPENDICES	50

LIST OF FIGURES

Figure 1. 1 Tanzania map showing location of stations used	6
Figure 3. 1 UNAVCO/EarthScope Consortium download manager	26
Figure 3. 2 Download option for RINEX data.....	27
Figure 3. 3 Downloading option for all RINEX data.....	27
Figure 3. 4 Uncrinexing hatanaked files using crx2rnx	28
Figure 3. 5 Meteorological Data download script	29
Figure 3. 6 Workflow for processing GNSS Data by using GAMIT Software	30
Figure 3. 7 Sh_gamit command for processing day 001	31
Figure 3. 8 A sample script showing processing for day 301 to 367.....	32
Figure 3. 9 Script showing processing for day 1 to 9 in utility sh_metutil.....	33
Figure 3. 10 Script showing processing for day 10 to 99	33
Figure 3. 11 Script showing processing for day 100 to 366	34
Figure 4.1 Graph showing ZHD trend at ARSH station.....	37
Figure 4.2 Graph showing ZHD trend at DODM station	37
Figure 4.3 Graph showing ZHD trend at MTVE station	38
Figure 4.4 Graph showing ZHD for points of different elevation	38
Figure 4.5 Graph showing ZWD trend at ARSH station	40
Figure 4.6 Graph showing ZWD trend at DODM station	40
Figure 4.7 Graph showing ZWD trend at MTVE station	41
Figure 4.8 Graph showing ZWD trends for points of different elevation	41
Figure 4.9 Graph showing ZTD trend for points of different elevation	43
Figure 4. 10 Graph shows error bar for ZTD values for points of different station	43

LIST OF TABLES

Table 2- 1 Coefficients for hydrostatic mapping functions	21
Table 2- 2 Coefficients for wet mapping functions	21
Table 3-1 Station used on the research	25
Table 4- 1 3D position of stations.....	35
Table 4- 2 Mean ZHD values of stations	36
Table 4- 3 Mean ZWD values for points of different elevation	39
Table 4-4 Mean ZTD values of stations	42

ACRONYMS AND ABBREVIATIONS

ZTD	Zenith Total Delay
ZHD	Zenith Hydrostatic Delay
GPS	Global Positioning System
GNSS	Global Navigation Satellite System
ZWD	Zenith Wet Delay
PWV	Precipitable Water Vapour
RTK	Real Time Kinematics
ANN	Artificial Neural Network
DD	Double differencing
PPP	Precise Point Positioning
CORS	Continuous Observing Reference Station
IWV	Integrated Water Vapour
UNAVCO	University NAVSTAR Consortium
SVs	Space Vehicles
PNT	Positioning Navigational and Timing
GIS	Geographical Information System
TMA	Tanzania Meteorological Agency
RINEX	Receiver Independent Exchange Format

CHAPTER ONE

INTRODUCTION

The tropospheric delay is a significant error source in GNSS positioning and navigation by approximately 10% to 20%. This is the delay of the signals as they propagate between the satellites and the user receiver. This delay is caused by the increased density of the troposphere. The delay is typically divided into wet and hydrostatic components. The total tropospheric delay is generally referred to as the zenith total delay (ZTD). Tropospheric delay can be problematic especially when stations are widely distributed at different altitudes. The signal in the atmosphere propagates slightly slower than in a vacuum; the refractive index of the troposphere is greater so it causes an excess delay of the GNSS signals (Acheampong, 2008).

Tropospheric delay can be expressed as a function of atmospheric pressure and temperature. Satellite signals travelling through the earth's atmosphere are refracted due to variation in the refractive index of the troposphere. This tends to bend the signals from their original path at varying heights. That is, the index is a function of the tropospheric path through which the signal passes from the receiver antenna to the end of the troposphere. This depends on temperature, pressure, humidity and the location of the GPS signal antenna. To provide feasible measurements of tropospheric delay, all the other error or perturbation sources must be estimated with precision. This parameter is computed in GPS processing through an integral quantity estimative in metric units along the zenithal direction for each chosen station. This estimate, defined as Zenith Total Delay (ZTD), is determined through all sets of slant path observations of delay (SD) from each station to all observed satellites in its horizon, forming an area on the troposphere roughly similar to a cone (Sickle, 2008).

Troposphere is the lowest part of the atmosphere closest to the earth's surface that extends from the surface about 9 km over the pole, 16 km over the equator and its total average thickness is about 13 km. It contains temperature pressure and humidity which are some of the constituents in the troposphere which affects the GNSS radio signals as they propagate through it. Troposphere thickness is not constant, it varies from place to place. These atmospheric temperature and pressure vary with height in which they decrease with increase

in altitude. The temperature decreases at a lapse rate which has significance on the GNSS observation that is conducted at different elevations. Previous research has shown that the ZTD is approximately 2.3 m, and approximately 90% of it is the zenith hydrostatic delay (ZHD). The ZHD can be estimated by measuring the surface pressure and temperature. Zenith wet delay (ZWD) accounts for approximately 10% and is mainly related to the water vapour content. The amount and properties of temperature pressure and humidity that contribute to the thickness of the troposphere and delays of GNSS signals can be classified as hydrostatic delay and wet delay (Pratap, 2006). Hydrostatic delay is made up of dry gases constituting about 90% of total delay.

Signals travel long distances at low elevation compared to high elevation since there are less delays in high elevation than low elevation. There are two zenith tropospheric delay which are divided into two components Zenith dry or hydrostatic delay (ZHD) and Zenith wet delay (ZWD)

1.0.1 Zenith dry or hydrostatic delay (ZHD).

The delay can be calculated with high accuracy using the surface pressure. It is due to the total mass of the atmosphere above the GPS antenna. ZHD accounts for about 90% of the ZTD and can easily be modelled or predicted to submillimeter accuracy by empirical prediction models using surface meteorological observations

1.0.2 Zenith wet delay (ZWD).

The ZWD accounts for the remaining 10% of the ZTD, and in contrast to the ZHD, it cannot be precisely modelled or predicted due to its large spatial and temporal variability. It depends on the water vapour along which the signal path and is weakly correlated with surface metrological data which limit its prediction accuracy. Since it depends on water vapour there are different ways to express water vapour content of the atmosphere which are Integrated Water Vapour (IWV) and Precipitable Water Vapour (PWV).

The zenith hydrostatic delay (ZHD) can be determined within a millimetre accuracy by empirical models. These models achieve deviations of up to about 20% in determining wet delay. The error in the zenith direction for the Saastamoinen model is approximately 0.2 mm for hydrostatic delay and 30 mm for wet delay. The determination of zenith wet delay (ZWD)

with a high spatial resolution is an important issue in meteorological estimation studies, as well as real-time positioning based on Global Navigation Satellite System (GNSS) observations. In the last decade, Continuously Operating Reference Station (CORS) networks have been established in many countries.

The Real Time Kinematic (RTK) method's positioning accuracy depends on the inter-station distances of the GNSS networks. The troposphere delay error reaches a few cm at distance of 70 km and above between the reference stations. In addition, tropospheric delay can cause errors in the height component up to several cm for RTK positioning. The error increases when the regional meteorological conditions notably change, and differences up to 3–4 cm may occur, depending on the season. The wet delay for any location can be accurately estimated with an effective interpolation method by using the surrounding GNSS station observations. In this way, a sufficient resolution and accuracy for meteorological forecasts can be achieved. Therefore, tropospheric error interpolation becomes more important, especially for sparse GNSS networks (Selbesoglu, 2019).

Spatial interpolation of the tropospheric wet delay is a difficult issue due to the rapid spatial variations of water vapor in the troposphere. Furthermore, the complexity of the physical structure of the atmosphere adversely affects interpolation methods designed without using meteorological parameters. Although different methods (IDW: Inverse Distance Weighted, LIM: Linear Interpolation Method, OK: Ordinary Kriging, etc.) have been presented for tropospheric interpolation in GNSS networks, it can be said that zenith wet delay interpolation is still a challenging issue, especially when inter-station distances increase. Therefore, the incorporation of meteorological parameters into the advanced models, such as the artificial neural network model, may enhance the interpolation performance.

The tropospheric delay for GNSS signals has been defined by mathematical models based on the relative humidity, pressure, and temperature meteorological parameters in various studies. On the other hand, ZWD caused by water vapor also depends on the weighted mean temperature of the troposphere. Therefore, the pressure, temperature, weighted mean temperature, and water vapor pressure were used as the input in the artificial neural network (ANN) model for spatial ZWD interpolation in the study. In this context, modelling and interpolation of the troposphere delay is of great importance for the field of GNSS meteorology, which has become an important field of research. Nowadays, artificial neural

networks have become a frequently used effective method for estimating meteorological parameters (Selbesoglu, 2019).

Many studies have been undertaken to improve the performance of ground-based GPS tropospheric delay estimation. (Schueler *et al*, 2000) compared the ZTD estimated from their spatial interpolation of the tropospheric delay method with the IGS ZTD and found an agreement of 1.7 cm. (Penna *et al*, 2001) compared the ZTD from the SBAS tropospheric model with that obtained from an analysis of one-year GPS carrier phase data analysed and published by (Dodson *et al*, 2000). They found that, for five stations in the United Kingdom, between 72% and 78% of the differences were <5 cm and between 96% and 99% were <10 cm. They also concluded that the RMS positioning errors in height component ranged from 4.0 to 4.7 cm, with maximum positioning errors ranging from 13.2 to 17.8 cm.

The study by (Njau, 2021) presented the determination of ZTD, ZHD, and ZWD whereby he used saastamoinen 1973 model to determine ZHD and g LAB software to determine ZTD as he established network of 9 point with different elevations and obtains points which are at high elevation (R6 1862m) has lower delay of 1.887 than point of lower elevation (R1 1711m) have large delay 2.047. this is because of variation of atmospheric pressure and temperature with height which contributes to delay in GNSS signal from the satellite to receiver.

This research aims to conduct an investigation into the Zenith Tropospheric delays (ZTD) experienced by three distinct geographical points (ARSH, MTVE, DODM) situated at varying elevations and climatic regions. By examining the influence of elevation disparities and diverse weather patterns on Zenith Tropospheric delays, this study aims to shed light on the combined effects of these factors.

1.1 Statement of the problem

As Global Navigation Satellite System (GNSS) signals travel through the troposphere, a tropospheric delay occurs due to a change in the refractive index of the medium. The GPS processing in order to determine the stations precise coordinates is interlinked with the GPS atmospheric processing to obtain the precise atmospheric parameters for those stations. Hence, to determine the station coordinates as accurately as possible, the GPS atmospheric delay needs to be identified and separated from the other errors and perturbations sources of the method. The troposphere is not constant as it varies from place to place due to its

components as temperature, pressure and humidity which are determining tropospheric delay. The tropospheric delay in measured distance typically in zenith is about 2.5m means troposphere may cause GPS observation to have additional distance error between receivers and satellites at zenith. So, this research intends to assess those calculated ZHD and ZWD from points of different elevation for accurate positioning with different elevation in which models can be used to mitigate those effects of tropospheric variation.

1.2 Main objective

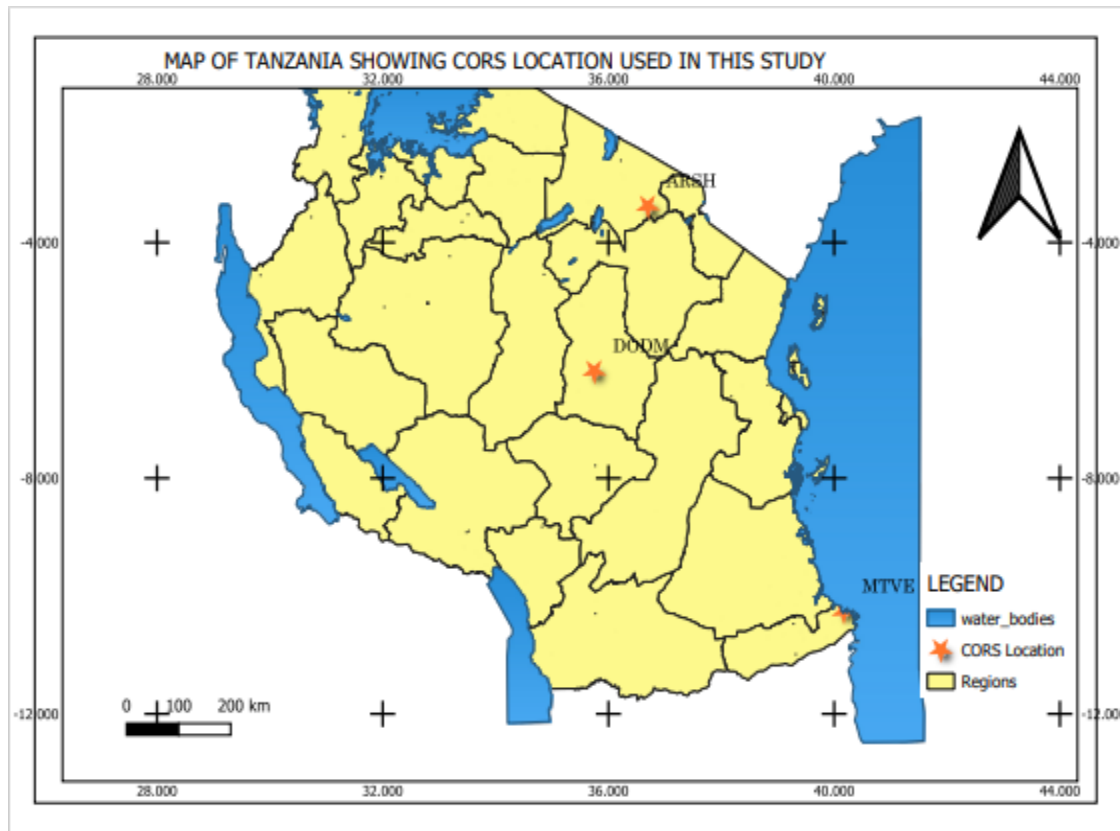
To assess the GNSS computed ZTD, ZHD, and ZWD for points of different elevation for accurate positioning with different elevation in which models can be used to mitigate those effects of tropospheric variation.

1.3 Specific objectives

- I. To assess amounts of delays computed of these points of different elevation
- II. To assess effect of climate variation and the amount of delays for these points

1.4 CORS locations used in this study

The study is about retrieving Zenith Tropospheric Delay (ZTD) for interval of 1 year (1st/Jan/2015-1st/Jan/2016) from GNSS CORS stations at Dodoma with station ID DODM located at latitude -6.187°S and longitude 35.748°E , at Arusha with station ID ARSH located at latitude -3.387°S and longitude 36.698°E and at Mtwara with station ID MTVE at latitude -10.26°S and longitude 40.166°E as shown on Figure 1.1. These stations they are grouped as Africa array/Met sites by UNAVCO.



(field work)

Figure 1. 1 *Tanzania map showing location of stations used*

1.5 Significance of the research

The society will be benefits from this research after finding those computed parameters and asses them to determine their accuracy. Also, On the other hand, ZTD corrections are also used to improved GNSS positioning. The research also stimulates the Geomatics students and other researches on doing more research related to atmospheric science by using their knowledge on GNSS technique and so increasing applicability of diversity of the course. GNSS-derived ZTD and ZWD data provide valuable information about the state of the atmosphere, particularly in terms of water vapor content. Accurate measurements of these parameters can significantly improve weather forecasting models and aid in climate studies, helping to better understand and predict weather patterns and extreme weather events like storms, hurricanes, and heavy rainfall. Also, they can identify factors and solution to tropospheric variation that contribute to reliable GNSS measurement at different altitude and by understanding the relationship between ZTD, ZWD, and ZHD at different

elevations can lead to the development of improved tropospheric correction models, enhancing the precision of GNSS data analysis and satellite positioning. Also, for monitoring climate change as long-term observations of ZTD and ZWD at different elevations can help monitor climate change patterns and their impact on the atmosphere's water vapor distribution. Changes in these parameters over time can offer insights into the Earth's changing climate and its potential consequences.

1.6 Scope and limitation

This study deals with assessment of computed ZTD, ZHD and ZWD for points of different elevation where by it only deals with tropospheric error. But there are other sources of error like clock error, cycle slip and ionospheric error that will be taken into account.

1.7 Organization of the study

The study is organised into five chapters. Chapter one present the introduction of the study which covers introduction statement of the problem, research objectives, scope and limitation of the study. Chapter two contains mainly literature review of related literatures which includes the definition of key terms. Chapter three presents the research methodology and procedures used for gathering data and data processing. Chapter four present the research results and analysis. Chapter five present conclusion and recommendations.

CHAPTER TWO

LITERATURE REVIEW

2.1 Global Navigation Satellite System

Is a system of satellite designed to provide autonomous geospatial positioning and timing information for user on earth and space, also it consists constellation of satellite orbiting the earth and continuously transmitting signals that enable the user to determine their 3D positioning with the global coverage. It is a system of satellite designed to provide autonomous geospatial positioning and timing information for users on earth and space, also it consists constellation of satellites orbiting the earth and continuously transmitting signals that enable the users to determine their 3D positions with the global coverage (Subirana et al., May 2013).

It consists of GPS(USA), GLONASS (Russia), Galileo (Europe), Beidou (China) for global coverage. But the other region systems such as IRNSS (India) and QZSS (Japan) which are not for global coverage but currently the most widely used operational GNSS is the GPS. It consists of 24 satellites in approximately 12-hour orbits, six different orbital planes that designed and realized by the U.S department of defence. Also, GPS has three segment which are space, user and ground control. The origin of GPS is in the sputnik era when the scientists were able to track the satellite with shift in its radio signal known as the "Doppler Effect". Today GPS is multi use, space-based radio navigation system owned by US government and operated by the United State Air force to meet the national defence.

2.1.1 Main principle of GNSS

The main principle behind a satellite navigation system is the creation of a trilateration from any point on the earth's surface to the satellites in view. The distance to the satellites is measured by the time the radio signal needs to reach the receiver. Because a radio signal travels with the speed of light, highly precise clocks are used. The satellites contain atomic clocks, and the receivers advanced quartz clocks. The distance to the satellite can be calculated by multiplying the travel time by the speed of light (approximately 300000 km/s). The exact location of the satellite in space is a prerequisite for this procedure. This is possible because the orbits are very stable and predictable (Lechner & Baumann, 2000).

The satellites are observed and controlled by ground stations, which put the spatial information into the signal. These are the so-called “ephemeris data” (orbit of one satellite) and “almanac data” (relation between all of the satellites). Additionally, information on the satellite clocks is transmitted. In principle, three satellites must be available to determine a three-dimensional position. All points, which have the same distance to one satellite, form a spherical surface with the satellite in the centre. Three spherical surfaces intersect in two points. One point can be disregarded, because its position is located too far from the earth. A fourth signal is necessary to eliminate the time difference between the satellite’s atomic clocks and the receivers’ quartz clocks. This technique allows the use of inexpensive clocks in user equipment (Lechner & Baumann, 2000).

Depending on receiver type and tracked signals GNSS usage at any instance depends on:

- i Line-of-sight conditions between user receiver and GNSS constellation
- ii Receivers Signal-to-Noise-Ratio (SNR) threshold for acquisition and tracking of GNSS signals.
- iii Receiver characteristic for high dynamic environment and the related Doppler frequency shift.

2.1.2 GNSS segments

All GNSS are composed of three (3) main segments: the space, control and user segments. A brief description is given below:

2.1.2.1 Space Segment

This segment is basically the space vehicles (SVs) or satellites and provide the platform for atomic clocks, radio transceivers, computers, solar panels for power supply and a propulsion system for orbit adjustments and stability control (Hofmann-Wellenhof et al., 2020). Its main functions are to generate and transmit code and carrier phase signals, and to store and broadcast the navigation message sent to it by the control segment (Misra & Enge, 2011).

2.1.2.2 Control Segment

The task of the Control Segment is to provide command and control functions in:

- i. Continuously monitoring the whole system
- ii. Controlling and maintaining the status and configuration of satellite system
- iii. Keeping the corresponding GNSS time scale
- iv. Predicting the satellite ephemerides and the behaviour of the satellite clocks
- v. Periodically updating the navigation message for all satellites in the constellation, and commanding small manoeuvres to maintain orbit, (Misra & Enge, 2011; Subriana *et al.*, 2014).

2.1.2.3 User segment

This is mainly the GNSS receivers and information services designed to report constellation status, scheduled outages, and orbital data. User receivers are used to track signals, determine observables (carrier phase, pseudo ranges and doppler), solve for navigation equations and compute accurate position, velocity and time (Misra & Enge, 2011). The basic components of GNSS receivers are: antenna, radio frequency section, microprocessor, power source, data memory storage and user control panel.

2.1.3 GNSS Signal and Observables

GNSS are passive one-way down-link satellite ranging systems emitting modulated signals that include the time of transmission to derive ranges as well as the modelling parameters to compute satellite positions at any epoch (Hofmann-Wellenhof *et al.*, 2020). GNSS space vehicles continuously transmit navigation signals at two or more frequencies in L band (Subriana *et al.*, 2014).

The fundamental observable is the signal travel time between the satellite antenna and the receiver antenna. The signal travel time is scaled into a range measurement using the signal propagation velocity. The observed signal travel time always contains a systematic synchronization error (time bias) due to different clocks on-board SVs and receivers (Misra & Enge, 2011). Hence ranges obtained from these time-biased signals are called pseudo ranges as they are more than the true geometric ranges. The detailed structures of the various GNSS signals can be found in Interface Control Documents published by system providers. The main signal components are identified as follows:

- i. Carrier: radio frequency sinusoidal signal at a given frequency
- ii. Ranging code: sequences of zeros and ones which allow the receiver to determine the travel time of the radio signal from the satellite to the receiver. They are called the PRN sequences or codes
- iii. Navigation data: a binary-coded message providing information on the satellite ephemeris, clock bias parameters, almanac, and satellite health status (Misra & Enge, 2011; Subriana *et al.*, 2014)

Observables in GNSS are categorized into four (4) parts

- i. pseudo ranges from code measurements
- ii. pseudo range differences from integrated Doppler counts
- iii. carrier phases or carrier phase differences, and iv. differences in signal travel time from interferometric measurements (Misra & Enge, 2011).

The fundamental observation equations for both code pseudo ranges and carrier phase as given by (Misra & Enge, 2011) showed below.

1. For code pseudo ranges, the basic measurement made by the GNSS receiver is the apparent transit time of the signal from satellite to receiver. The value obtained is biased due to non-synchronized clocks of the satellite and receiver clocks, atmospheric propagation delays and environmental effects, hence the name pseudo ranges.

$$\rho(t) = R + c [\delta t_r - \delta t_s] + I_\rho + T_\rho + \varepsilon_\rho \dots\dots\dots \text{Eq (2.1)}$$

where, ρ , is pseudo range, R is the true range, I_ρ and T_ρ are the delays associated with signal transmission through the ionosphere and troposphere delays, ε_ρ are measurement noise, c is speed of light in vacuum, $(\delta t_r - \delta t_s)$ are receiver and satellite clock biases respectively.

2. For carrier phases the receiver measures the difference between the phases of the receiver-generated carrier signal and the carrier received from satellites at the instant of the measurement. For carrier phases to be measured, the receiver needs to acquire phase lock with the satellite signal, measures the initial fractional phase difference,

count full cycles and tracks changes of the fractional cycle at each epoch (Misra & Enge, 2011). The carrier phase is given as:

$$\varphi = \lambda^{-1}[R + I_{\rho} + T_{\rho}] + \frac{c}{\lambda} [\delta t_r - \delta t_s] + N + \varepsilon_{\rho} \dots\dots\dots \text{Eq (2.2)}$$

where, φ , is carrier phase, λ is wavelength, N is integer ambiguity. The fundamental difference between both observables is the ambiguity term (N) in carrier phase observation.

2.1.3 GNSS applications

The applications scope of GNSS ranges from simple, single benefits for individual users, to enormous, multifaceted benefits for nations of the world (Acheampong, 2008). These varied resources and different approaches to use signal-in-space for Positioning Navigational and Timing (PNT) applications are motivated by the fact that GPS and GLONASS were originally military systems and can be switched off by system providers in times of combat. With this information, nations are developing systems to retain their navigational capabilities that will not solely be reliant on one GNSS. A more technical motivation is in the combination of multiple signals from different GNSS as a single failure can result in a denial of service to a large number of users (Acheampong, 2015). GNSS signals transmitted from satellites in known orbits and tracked by users are used to generate an estimate of position, velocity and time, which gives it a different application including:

- i. Land, Sea and Air Navigation and Tracking: - including way-points as well as precise navigation, collision avoidance, cargo monitoring, vehicle tracking, search and rescue operations, etc.
- ii. Surveying and Mapping, on land, at sea and from the air. Includes geophysical and resource surveys, GIS data capture surveys, engineering and topographic surveys, etc.
- iii. Military Applications: the military systems are generally developed to “military specifications” and a greater emphasis is placed on system reliability and increased power against interference and jamming.
- iv. Recreational Uses on land, at sea and in the air.

- v. Timing and Frequency settings: - With the systems' accurate time references, GNSS-based time are used for the synchronization of very accurate clocks and timing standards¹. Notable uses are in the control of data communications networks, synchronized switching of power grids and timing of race cars.
- vi. Scientist applications: These include using signals for remote sensing of the environment, space weather studies, altitude determination, spacecraft operations
- vii. Other specialised uses are movement of the Earth's Crust, precision agriculture, environmental/crisis management.

2.1.4 GNSS positioning techniques

With the right receiver users have access to the four different observables provided by GNSS thus making it possible to use the signals in a variety of configurations for user satisfaction (Acheampong, 2015).

All GNSS are designed to offer two levels of positioning services; the highly accurate service, which is available only to authorized users, and a Standard Positioning Service (SPS), a less accurate positioning and timing service which is available to all users (ROB-Editors, 2016). From the SPS, Position, Velocity and Timing (PVT) solutions can be derived by using the receivers in either autonomous or relative modes.

2.1.4.1 Autonomous or Single Point Positioning

Involves the use of only a single GNSS receiver to collect data from multiple satellites in order to determine the user's geographical position and navigational output based the GNSS referenced frame. The performance of stand-alone GNSS is sufficient only for a limited number of applications especially those requiring lower accuracies (Acheampong, 2015). Centimetre-level accuracies are achievable when carrier phase measurements from dual frequency receivers are combined with precise orbits and satellite clock corrections products from IGS servers (Ghoddousi-fard & Dare, 2006).

This makes autonomous positioning to be further categorized into Standard point positioning (SPP) which uses pseudo range and broadcast ephemeris to determine absolute position of a receiver and Precise Point Positioning (PPP) which uses highly precise satellite clock and orbit information by least squares solutions. PPP technique is similar to Single Point

Positioning (SPP) in the sense that both techniques use pseudo range. However, PPP technique differs from the SPP because the latter neither uses precise ephemerides nor precise carrier phase data. PPP technique is one which has been used in this research as it contains some advantages over Relative technique that is no need to have more than one station and knowledge of receiver position is not a mandatory requirement.

2.1.4.2 Relative or Differential Positioning

This requires at least two receivers set up at more than one station (with at least one location known) to observe/measure satellite data simultaneously in order to determine coordinate differences. This method positions the receivers relative to each other and provides improved accuracies. It can also be described as a process of determining the relative differences in coordinates between two receiver points, each of which is simultaneously maintains lock unto satellites measuring code ranges and/or carrier phases from GNSS constellations (USACE-Editors, 2003).

The reference station calculates corrections which are transmitted to the remote receiver in real time via a data link or stored to be applied later. Differential systems give better accuracies than stand-alone positioning modes and also provide information on the position integrity (USACE-Editors, 2003). Differential techniques are further classified, depending on the status of the rover receiver and the period of observation as static, fast-static, kinematic or real-time kinematic (RTK). Its design can be implemented from local, regional or global areas.

2.2 GNSS Error Sources

Refers to all obstructions that makes difficult for GNSS receiver to calculate the accurate positions (Mohindre *et al.*, 2013). Since any measurements are associated with errors so these are the factors that make difficult for a GNSS receiver to calculate the exact position,

2.2.1 Tropospheric errors

The troposphere is the electrically neutral atmospheric region that it extends up to about 50km from the surface of the earth (Sickle, 2008). This layer is non-dispersive medium for the radio frequencies below 15GHz1 that's mean that is frequencies independent. So that the measured satellite to receiver range will be longer than the actual geometric range, which means that the distance between two receivers will be longer than the actual distance

(Diggelen, 2009) . This the deviation of the actual distance is caused by the delays in the troposphere which depend on the temperature, pressure and humidity along the signal path through the troposphere (Hofmann-Wellenhof *et al.*, 2020).

2.2.1.1 Tropospheric delay

Tropospheric layer also refracts GNSS signals, unlike the ionosphere, it is non-dispersive for radio waves (i.e., the refractive index is independent of the signals' frequency) (Acheampong, 2015). Measurements of code and carrier phases at the various frequencies experience a common delay (Misra P. &, 2011). The tropospheric medium slows the speed of propagation of the signal making range measurements to satellites longer. The earth's atmosphere affects microwave or radio signals passing through it in three ways: it causes propagation delays; it causes ray bending; and signal absorption (Kleijer, 2004).

Propagation delays and ray bending effects on the neutral atmosphere were considered for this study and from literature the total delays depend on the refractivity along the travelled path (Solheim). This refractivity is a function of pressure and temperature at the receiving station. From Fermat's principle and following (Kleijer, 2004). The geometric distance of ray is given by:

$$L = \int_l dl \dots\dots\dots Eq (2.3)$$

where L is the geometrical distance and l is geometrical path. The excess path length becomes

$$\Delta L_a^i(\epsilon) = S - L = \int_s (n(s) - 1)ds + \{\int_s ds - \int_l dl\} \dots\dots\dots Eq (2.4)$$

Where is excess path length (Delay) in the slant direction for a signal from satellite, i to receiver's antenna, a , at elevation angle, ϵ . $\int_s (n(s) - 1)ds$ on the right-hand side is the excess path length caused by the propagation delay $\int_s ds - \int_l dl$ and is the excess path length caused by ray bending. The aspects caused by ray bending are negligible at higher 29 satellite elevations based. The tropospheric effects can introduce errors from 2.5 m to as high as 25 m depending on the elevation of the satellite (Seeber, 2003). $\Delta dtrop$, cannot be estimated from GNSS observables and as such its effects are mitigated by using models. $\Delta dtrop$ on range measurements to satellites are made up of two components: the dry component and the wet component. Hence, $\Delta dtrop$ can further be defined as:

$$\Delta d_{trop} = \Delta d_{tropd} + \Delta d_{tropw} \dots \dots \dots Eq (2.5)$$

where, Δd_{tropd} is the dry or hydrostatic component and Δd_{tropw} is the wet component. Δd_{tropw} , which comprises only 10% of total tropospheric refraction, depends on the distribution of water vapour in the atmosphere and the harder of the two components to model (Seeber, 2003).

Whereby, Δd_{tropd} can be precisely described within an accuracy of $\pm 1\%$ by tropospheric models. Wet delays on the other hand, according to can be modelled using precise surface meteorological parameters with an accuracy not better than 2cm. Models for tropospheric refraction are based on functions of meteorological parameters and refractive index of air mass along signal path (Acheampong, 2015). An empirical formula for computing the reduced index of tropospheric refraction, N , and $N(s)$ is given below:

$$N = k_1 \frac{p_d}{T} Z_d^{-1} + k_2 \frac{e}{T} Z_w^{-1} + k_3 \frac{e}{T^2} Z_w^{-1} \Rightarrow N(s) = [n(s) - 1] 10^6 \dots \dots \dots Eq (2.6)$$

where p_d and e are partial pressures of the dry gases and water vapour in hPa, T is absolute temperature in Kelvin's; and are inverse are compressibility factors for dry and moist air respectively and are used to describe the deviation of the atmospheric constituents from an ideal gas; k_1 , k_2 and k_3 are constants based on laboratories estimates and their values were found to be $k_1 = 77.60 \pm 0.05$ K/hPa, $k_2 = 77.40 \pm 2.2$ K/hPa, $k_3 = 373900 \pm 1200$ K² /hPa and $k'_2 = 22.10 \pm 2.2$ K/hPa (Bevis, 1994).

Eq (2.17), can further be expressed in terms of integrals of the two components and ignoring all other terms which are zero in the zenith direction, becomes:

$$\Delta d_{trop} = 10^{-6} \int_{atm} N(s). ds = \int_{atm} [\Delta d_{tropd}(s) + \Delta d_{tropw}(s)]. ds \dots \dots \dots Eq (2.7)$$

Most tropospheric delays estimations are based on average meteorological conditions at the antenna location from models of the standard atmosphere using the day of the year, latitude and altitude (Misra & Enge, 2011). Two approaches that are used to estimate Δd_{trop} are: Estimation of the Zenith tropospheric delay (ZTD) in terms of the corresponding dry (ZHD) and wet delays (ZWD);

$$ZTD = ZHD + ZWD \dots \dots \dots Eq (2.8)$$

2.2.1.2 Zenith tropospheric delays

Tropospheric delay can be problematic, especially when the stations are widely distributed at different altitude (Awange, 2012). For examples cold (dense air) can accumulate in mountain basins on clear calm nights whilst mountain tops may be considerably warmer. The signal in the atmosphere propagates slightly slower than in a vacuum, the refractive index of the troposphere is greater so it causes an excess delay of the GNSS signals. The tropospheric delay is directly proportional to the refractive index, the tropospheric delay can be expressed as a function of the atmospheric temperature and pressure (Subriana *et al.*, 2014).

These delays are measured in zenith direction in which are estimated to be 2.3m at sea level and it increases near the horizon or the earth surfaces (there is no signal bending in zenith direction). There are two zenith tropospheric delays which are divided into two components which are the following mentioned below.

a) Zenith dry or hydrostatic delay

This delay is due to the total mass of the atmosphere above the GPS antenna. The dry component Contributes about 90% of the total delay and can be predicted to a high degree of accuracy using mathematical models (Sickle, 2008). This caused by the dry gases and particles can be precisely determined from the surface measurement using empirical models which are Saastamoinen, 1973 and Hopfield 1971.

The dry delay can be modelled by employing surface and ground meteorological data or by acquiring them from the external or internal sources such NCEP, ECMWF and TMA. Some receivers have the utilization of the standard atmospheric models for calculated of the related weather parameters (Shrestha, 2013) . This delay sometimes known as zenith hydrostatic delay and denoted as ZHD.

b) Zenith Wet delay

The wet delay is small than the dry delay approximately to be 10% of the total delay and is more variable and difficult to remove because it varying with time and space (Rabbany, 2002). It depends on the water vapour along which the signal path and is weakly correlated with the surface meteorological data which limit its prediction accuracy (Rabbany, 2002). It was found that using default meteorological data (1010mb for atmospheric pressure, 20°C for temperature and 50% for the relative humidity) give satisfactory result in most cases. Since it

depends on the water vapour, there are different ways to express the water vapour content of atmosphere which are Integrated Water Vapour (IWV) and precipitable water vapour (PWV). These delays it denoted as ZWD and the value of PWV is obtained by multiplying ZWD by the constant k approximately to be 0.15 (Reguzzoni, 2013). So that, the total zenith tropospheric delay (ZTD) is obtained by the sum of zenith wet delay (ZWD) and zenith hydrostatic delay (ZHD).

In total, 90% of the total tropospheric delay is due to the dry (hydrostatic) component. The troposphere delay caused by the hydrostatic component is 2.3 m on average. The calculation of the hydrostatic delay can be calculated precisely by using pressure measurements at the station location based on troposphere delay models. Afterwards, the calculated value is assumed to be the default value for ZWD estimation by GNSS measurements, and the ZWD is estimated by the least square adjustment method. In this estimation, the accuracy of the ZHD value calculated as the preliminary value is important for the accuracy of the estimation of the ZWD. The accuracy of the ZHD value is directly related to the accuracy of pressure measurements. A 1 hPa error in pressure measurements (Selbesoglu, 2019).

There are various models that are used to estimate the of ZWD and ZHD, where by the sum of them is ZTD. These models are like Saastamoinen 1972 and Hopfield model. The mostly model used is Saastamoinen 1972 tropospheric model

2.2.1.3 Saastamoinen model

Saastamoinen (1972) applied the gas laws to refractivity by considering the atmosphere as a mixture of dry air and water vapour. The model considers the temperature in the troposphere as decreasing with increasing height at a uniform rate, which varies slightly with latitude and season. However, in the polar region, there is a permanent inversion in the lower troposphere where the actual temperature increases with height. Saastamoinen assumed the neutral atmosphere to consist of two layers: the polytropic troposphere, which extends from the earth's surface to an altitude of approximately 11-12 km and the stratosphere, which is an isothermal layer, extending to approximately 50 km. The atmospheric water vapour is confined in the region of the troposphere only (Combrinck, 2015). The Saastamoinen model for ZHD, in metres, is expressed as:

$$ZHD = \frac{0.0022768p}{g} \dots\dots\dots \text{Eq (2.9)}$$

$$\text{Or } ZHD = \frac{2.2779 \pm 0.0024(mm).Ps}{1 - 0.00266.\cos\psi - 0.000289\left(\frac{1}{KM}\right).h} \dots\dots\dots \text{Eq (2.10)}$$

In the zenith wet delay model, Saastamoinen (1972) assumed that there is a linear decrease of temperature with height, and that the water vapour pressure decreases with height. The variation of the water vapour pressure e , (mbar) is expressed by the following expression:

$$e_x = RH \times 6.11 \times 10^{\frac{7.5T_s}{T_s + 273.15}} \dots\dots\dots \text{Eq (2.11)}$$

In Equation (1.3), RH is the relative humidity to be determined from local observations, and the surface temperature in Kelvin is T_s .

$$ZWD = \frac{0.0022768 \times 1255e}{(T + 273) + 5 \times 10^{-2}} \dots\dots\dots \text{Eq(2.12)}$$

Where by

P = pressure of station H = Height of station g

= local gravity acceleration of station height

e = Partial water vapour

ψ = latitude of station

T = estimated atmospheric temperature in K

2.3 Mapping Functions

Mapping functions is defined as the ratio of electric path through the atmosphere at geometric elevation ε to path in zenith direction. Mapping functions (also referred to as obliquity factors) are models used to convert the slant tropospheric delays to zenith delays. These functions make computations of total tropospheric delays easier as signals arrive at the antenna location from various angles (Acheampong, 2015). The simplest model for both dry (hydrostatic) and wet delays according is $1/\sin \text{el}$ works well when the earth is considered to be flat and satellites are above 15° elevation angles (el) (Misra & Enge, 2011). Several models have been developed to counter the effects of the earth's curvature and low-elevation satellites.

Below is the model which is based on a modified Niell (1996) model using the Marini (1972) model normalized to unity at the zenith (Niell, 1996; Ramos-Bosch, 2019). The models are presented below, where E is the elevation angle and H is receiver's height above sea level in km.

Hydrostatic mapping function:

$$M_{dry}(E, H) = m(E, a_d, b_d, c_d) + \Delta m(E, H) \dots\dots\dots \text{Eq (2.13)}$$

$$\text{With, } \Delta m(E, H) = \left[\frac{1}{\sin E} - m(E, a_{ht}, b_{ht}, c_{ht}) \right] \cdot H$$

Wet mapping function

$$M_{wet}(E, H) = m(E, a_w, b_w, c_w) \dots\dots\dots \text{Eq (2.14)}$$

$$\text{With } m(E, a, b, c) = \left[\frac{1 + \frac{a}{b}}{\sin E + \frac{a + \frac{1+c}{a}}{\sin E + \frac{b}{\sin E + c}}} \right]$$

Following (Subriana et al., 2014) and (Niell, 1996) the hydrostatic parameters a_d , b_d , c_d are time (t) and latitude (θ) dependent and can be evaluated using the expression

$$\xi(\theta, t) = \xi_{avg}(\theta) - \xi_{avg}(\theta) \cos \left(2\pi \frac{t - T_0}{365.25} \right) \dots\dots\dots \text{Eq (2.15)}$$

where t is the time from January 0.0, in days, and T_0 is taken as Day of Year (DoY). The parameters $\xi_{avg}(\theta)$ and $\xi_{avg}(\theta)$ are linearly interpolated from Table 2-1 using a_{ht} , b_{ht} , c_{ht} as constants. On the other hand, the wet components, a_w , b_w , c_w , are only dependent on latitudes and the linear interpolations are done using values from Table 2-2.

Table 2- 1 Coefficients for hydrostatic mapping functions

Coefficient (ξ)	Latitude (θ)				
	15°	30°	45°	60°	75°
Average					
a	1.2769934e-3	1.2683230e-3	1.2465397e-3	1.219604e-3	1.2045996e-3
b	2.9153695e-3	2.9152299e-3	2.9288445e-3	2.9022565e-3	2.9024912e-3
c	62.61055e-3	62.837393e-3	63.721774e-3	63.824265e-3	64.258455e-3
Amplitude					
a	0.0	1.2709626e-5	2.652366e-5	3.4000452e-5	4.1202191e-5
b	0.0	2.1414979e-5	2.6523662e-5	7.2562722e-5	11.723375e-5
c	0.0	9.0128400e-5	3.0160779e-5	84.795348e-5	170.37206e-5
Height Correction					
a_{ht}	2.53e-5				
b_{ht}	5.49e-3				
c_{ht}	1.14e-5				

(Subriana *et al.*, 2014)

Table 2- 2 Coefficients for wet mapping functions

Coefficient (ξ)	Latitude (θ)				
	15°	30°	45°	60°	75°
a	5.8021897e-4	5.6794847e-4	5.8118019e-4	5.9727542e-4	6.1641693e-4
b	1.4275268e-3	1.5138625e-3	1.4572752e-3	1.5007428e-3	2.9024912e-3
c	4.3472961e-2	4.6729510e-2	4.3908931e-2	4.4626982e-2	64.258455e-2

(Subriana *et al.*, 2014)

2.3.1 ZWD from total zenith tropospheric delay

From the equation of state for ideal gases, $p_d/T = R_d \rho_d$, where, R_d is the specific gas constant of the dry constituent, ($R_d = R/M_d$, R is the universal gas constant and M_d is the molar mass of the dry gases). Using simple approximations and the assumption of hydrostatic equation

being valid for total pressure and not for partial pressures, Davis et al. (1985) reformatted Eq (2.6) to be:

$$N = k_1 R_d \rho + k'_2 \frac{e}{T} + k_3 \frac{e}{T^2} \dots\dots\dots \text{Eq (2.16)}$$

k'_2 which has been given earlier is derived by the expression $k'_2 = k^2 - (M_w/M_d) k_1$, where M_w is the molar mass of water vapour; ρ is the total density of dry air and water vapour.

When all the slant delays are mapped onto the zenith direction, zenith hydrostatic delays, ZHD can be obtained by considering the assumption that hydrostatic equilibrium have been satisfied (Davis et al., 1985);

$$\frac{dp}{dh} = -p(h)g(h) \dots\dots\dots \text{Eq (2.17)}$$

where g is the acceleration due to gravity in the vertical direction; p is the total pressure.

The resultant integration of the first term in Eq (2.14) gives:

$$ZHD = (10^{-6} k_1 R_d g_m^{-1}) * P_s \dots\dots\dots \text{Eq (2.18)}$$

where P_s is the total ground pressure in hPa, g_m is gravitational acceleration at the mass centre of a vertical column of the atmosphere and $g_m = (9.784 \pm 0.001 \text{ m/s}^2) \cdot f(\theta, H)$, and

$$f(\theta, H) = (1 - 2.66 * 10^{-3} * \cos(2\theta) - 2.8 * 10^{-7} H) \dots\dots\dots \text{Eq (2.19)}$$

(Bevis, 1994).

The parameters θ and H are the latitude of the site in degrees and surface height above the geoid in meters respectively.

Substituting all the constants in Eq (2.16), the expression for solving ZHD in units of length become

$$ZHD = 0.002277(1 + 0.0026 \cos 2\theta + 0.00028H) \cdot P_s \dots\dots\dots \text{Eq (2.20)}$$

With ZTD already computed and knowledge of the precise coordinates of the antenna position. (θ, H) and surface pressure values from meteorological file or nearby weather station, ZWD can be computed using Eq (2.8) and Eq (2.20).

2.4 Related studies

Many studies have been undertaken to improve the performance of ground-based GPS tropospheric delay estimation. (Schueler *et al*, 2000) compared the ZTD estimated from their spatial interpolation of the tropospheric delay method with the IGS ZTD and found an agreement of 1.7 cm. (Penna *et al.*, 2001) compared the ZTD from the SBAS tropospheric model with that obtained from an analysis of one-year GPS carrier phase data analysed and published by (Dodson *et al.*, 2000). They found that, for five stations in the United Kingdom, between 72% and 78% of the differences were <5 cm and between 96% and 99% were <10 cm. They also concluded that the RMS positioning errors in height component ranged from 4.0 to 4.7 cm, with maximum positioning errors ranging from 13.2 to 17.8 cm.

(Njau, 2021) presented the determination of ZTD, ZHD, and ZWD whereby he used saastamoinen 1973 model to determine ZHD and g LAB software to determine ZTD as he established network of 9 point with different elevations and obtains points which are at high elevation (R6 1862m) has lower delay of 1.887 than point of lower elevation (R1 1711m) have large delay 2.047. this is because of variation of atmospheric pressure and temperature with height which contributes to delay in GNSS signal from the satellite to receiver.

(Leandro, 2006) presented and tested the UNB3m model as a modified version of the UNB3 model. They found that the predicted errors of the estimate of tropospheric delay from UNB3m had a mean value -0.5 cm and a standard deviation (STD) of 4.9 cm with respect to ray-tracing analysis. Furthermore, the treatment of the ZWD as a stochastic parameter, updated at every observation epoch in a Kalman filter, was found by (Pany *et al.*, 2007) to be a good tool with which to account for the high variability of the wet troposphere. (Pace *et al.*, 2010) presented a method for estimating ZTD residual fields using a ground-based GPS network. They modelled the zenith hydrostatic delay (ZHD) as an exponential function of latitude, whereas the ZWD was estimated every 5 minutes using a random walk stochastic model with a constraint of $20 \text{ mm}/(\sqrt{h})$. They found that the ZTD residuals were of the order of 50–100 mm.

The results presented by (Li *et al*, 2012), from 125 IGS stations during 2001-2005, summarized the magnitude of the bias and RMS of the differences between IGS ZTD and the estimated ZTD for the SBAS model (bias: 2.0 cm, RMS: 5.4 cm), UNB3 model (bias 2.0 cm, RMS: 5.4

CHAPTER THREE

METHODOLOGY

These are specific procedures or techniques used to identify collect select process and analyse the data used in this study. It allows critically evaluate a study's overall validity and reliability, and shows how data used in this study were collected and analysed. Data were downloaded and then processed by using GAMIT/GLOBK software in order to obtain desirable result for this study. In which plots of graphs were used to present and analyse data. The following are the steps and procedures used to collect and analyse data used in this study

3.1 Data Source and Acquisition

The study is based on three stations of different elevations as shown on the table 3-1.

Table 3-1 Station used on the research

STATION	Height
ARSH	1345.161
DODM	1122.595
MTVE	-11.414

Data used from the stations on this research were acquired from different international sources and different formats as explained below;

3.1.1 RINEX observation, meteorological, navigation files for experiment sites and RINEX observation files for IGS sites.

RINEX observation, meteorological and navigation files for the experiment site DODM and all IGS sites were downloaded from UNAVCO/EarthScope Consortium archives with the help of DAIV2 (Data Archive Interface version 2) with link <https://www.unavco.org/data/gps-gnss/data-accessmethods/dai2/app/dai2.html> and unavcoDownloadManager_v2 which gives a simplified graphical user interface large amount data downloading from UNAVCO/EarthScope Consortium. The IGS sites which were downloaded includes ABPO, ADIS, ACRG, ASCG, DARK, DEAR, HARB, MAL2, MSA1, NKLK, YKRO, ZAMB, SUTH, NKLK, SEY, REUN,

MBAR These files were downloaded covering each day of year for the specified interval with exception to days in which receivers were off.

All downloaded data from UNAVCO/EarthScope Consortium were in compressed format (.z) and furthermore, RINEX observation files were first crinexed (hatanaked(.d)). The data format RINEX observation, meteorological and navigation files were xxxddds.yyd.z, xxxddds.ym.z and xxxddds.yyn.z respectively in which xxxx is station marker name, ddd is day of year, s is session, yy are last two digits of year, d,n,m are file types. Figure 3.1, 3.2, and 3.3 shows the procedures to download RINEX data from UNAVCO/EarthScope Consortium download manager. Where by figure 3.1 is to search for station needed then after finding it figure 3.2 shows download option and for figure 3.3, we choose bundle of data for the data required was for some period of time.

Data Archive Interface v1

The screenshot displays the 'Permanent Stations' interface of the UNAVCO/EarthScope Consortium download manager. At the top right, there are links for 'Please provide feedback' and 'Printable View'. The main interface has a tabbed menu with 'Station Search' selected, alongside 'Temporal Search', 'Spatial Search', 'Monument/Equipment Search', 'Map Display', 'Tabular Display', 'Help', and 'Minimize'. Below the tabs, there are three main filter sections: 'Filter by 4-char Station Code List' with a text input and a list of station codes (e.g., 1LSU - Louisiana State University, 1NSU - Northwestern State University, 1ULM - U of Louisiana-Monroe, 299C - 2999 Continuous, 34A1 - 34A1, 34A2 - 34A2, 34A3 - 34A3, 34A4 - 34A4, 34NO - 34NO, 34SO - 34SO, 70AK - 70AK, 70DM - Seven Oaks Dam 1HZ); 'Filter by Network' with a 'Contains' dropdown and radio buttons for 'Contains' and 'Equals'; and 'Filter By Operational Status' with checkboxes for 'Active', 'Inactive', 'Retired', 'Pending', and 'Intermittent 5Hz or 1Hz'. At the bottom left, there are 'View Results' and 'Reset' buttons.

Figure 3. 1 UNAVCO/EarthScope Consortium download manager

Results 1 to 1 of 1 for ARSH, AFRICA ARRAY, Operational Status ACTIVE, Operational Status INACTIVE, Operational Status RETIRED, Operational Status PENDING

Click on an underlined column heading to sort. The sort order toggles between ascending and descending.

Currently, data is available on a per station basis. To access a station's data download options, please press the 'Download Options' button located in the Station Data column below.

<u>Station Code</u> ^	<u>Latitude</u>	Station Data	<u>Station Name</u>	<u>Earliest Data</u>	<u>Latest Data</u>
<u>Longitude</u>					
ARSH	3.387° S	Download Options	Arusha Ministry of Energy and Minerals	2013 Feb 27	2017 Mar 28
Summary	36.698° E				

1

Figure 3. 2 Download option for RINEX data

ARSH - Data Download Options					
<< Back to ARSH Search Result Page					
NOTICE - By downloading data from GAGE, you are agreeing to abide by the acknowledgments section of the GAGE Data Policy .					
Data Type	Estimated File Count	Estimated File Size	Start Time	End Time	Choose Option
Download Option					
RINEX Data					
All RINEX Data Individual File Links (hatanaka_obs_nav_gc)	1489	~1489MB	2013-02-27	2017-03-28	Bundle Data
Time-Windowed RINEX Data (To set a time window, use the browser back button and select the Temporal Search tab')			not selected	not selected	not selected
Latest RINEX Data File	1	~1MB		2016 Oct 30 23:59:45	Download

Figure 3. 3 Downloading option for all RINEX data

3.1.2 Precise ephemeris and precise clock files

The final satellite position files (precise ephemeris) in sp3 format and precise clock files in clk format were downloaded from data archives covering the interval specified above by corresponding the GPS week and day. These Data ranging from GPS day 001 to 365 And GPS week 1825 to 1877 of 2015. precise ephemeris files were downloaded using get_orb command with help of GAMIT/GLOBK software from data archives of cddis and corresponding clock files were downloaded through file transfer protocol (ftp) from cddis with the link <ftp://cddis.gsfc.nasa.gov/pub/gps/products/>.

The downloaded precise ephemeris and clock files were in cccwwd.sp3.z and cccwwd.clk.z respectively in which ccc-three letter ID for the centre which generated the file wwwfour digits GPS week d-single digit day of week 0=Sunday,

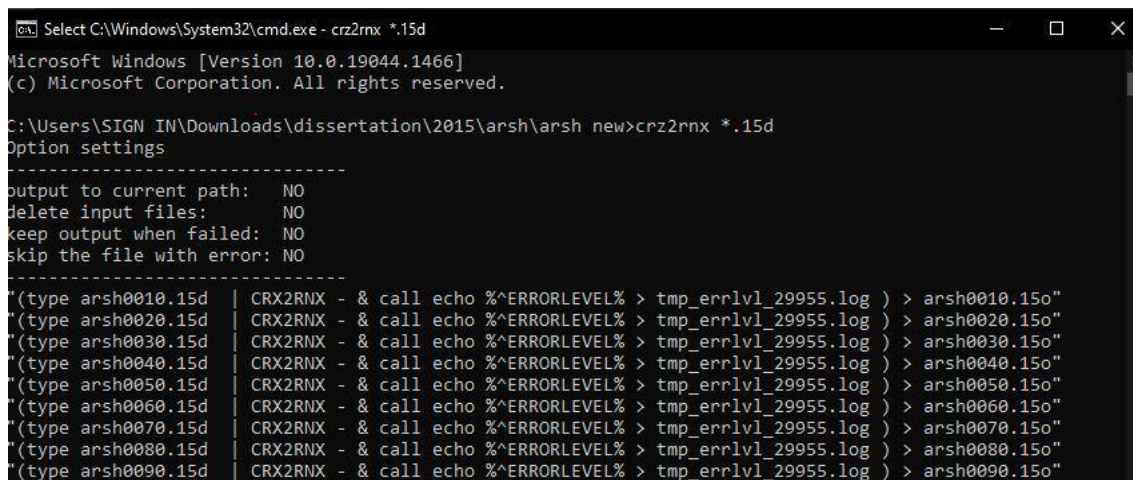
1=Monday...6 sp3/clk-file type.

3.2 Data preparation

The acquired data were prepared so as to meet requirements of specific task in need to accomplish this research objective. Data were manipulated in terms of changing their file type (extension), arranging them, finding mean and extracting them from different format so as they can be read by software under research.

3.2.1 RINEX observation files for experiment and IGS sites.

Observation files of all stations were acquired in compressed and crinexed format (xxxxddd.yy.d. z), and so data were first uncompressed using windows winRAR app to remove .z and then the hatanaked file (xxxxddd.yy.d) was uncrinexed to get xxxddd.yy.o observation files by using CRX2RNX_4.08 app in windows command line as shown in Figure 3-4.



```
Select C:\Windows\System32\cmd.exe - crx2rnrx *.15d
Microsoft Windows [Version 10.0.19044.1466]
(c) Microsoft Corporation. All rights reserved.

C:\Users\SIGN IN\Downloads\dissertation\2015\arsh\arsh new>crx2rnrx *.15d
Option settings
-----
output to current path: NO
delete input files: NO
keep output when failed: NO
skip the file with error: NO
-----
(type arsh0010.15d | CRX2RNX - & call echo %^ERRORLEVEL% > tmp_errlvl_29955.log ) > arsh0010.15o"
(type arsh0020.15d | CRX2RNX - & call echo %^ERRORLEVEL% > tmp_errlvl_29955.log ) > arsh0020.15o"
(type arsh0030.15d | CRX2RNX - & call echo %^ERRORLEVEL% > tmp_errlvl_29955.log ) > arsh0030.15o"
(type arsh0040.15d | CRX2RNX - & call echo %^ERRORLEVEL% > tmp_errlvl_29955.log ) > arsh0040.15o"
(type arsh0050.15d | CRX2RNX - & call echo %^ERRORLEVEL% > tmp_errlvl_29955.log ) > arsh0050.15o"
(type arsh0060.15d | CRX2RNX - & call echo %^ERRORLEVEL% > tmp_errlvl_29955.log ) > arsh0060.15o"
(type arsh0070.15d | CRX2RNX - & call echo %^ERRORLEVEL% > tmp_errlvl_29955.log ) > arsh0070.15o"
(type arsh0080.15d | CRX2RNX - & call echo %^ERRORLEVEL% > tmp_errlvl_29955.log ) > arsh0080.15o"
(type arsh0090.15d | CRX2RNX - & call echo %^ERRORLEVEL% > tmp_errlvl_29955.log ) > arsh0090.15o"
```

Figure 3. 4 *Uncrinexing hatanaked files using crx2rnrx*

3.2.2 RINEX navigation files

Navigation files with satellite information were also acquired in compressed format (xxxxddd.yyn.z), and so they were uncompressed using windows winRAR app to remove .z from files. The resulting files duplicated and one part was then renamed so as they can be read by GAMIT/GLOBK as brdc in station name of navigation file (xxxxddd.yyn→brdcdddd.yyn)

3.3 RINEX meteorological file

Meteorological Data were downloaded from UNAVCO where by the script for download is as shown on figure 3.5.

Powershell (WINDOWS, file explorer in this directory):

~~~~~

1. Right click download\_data.ps1 and choose "Run with PowerShell"
2. Enter the location to save the files in, such as Downloads, Documents, or Documents\folder\_name.
3. Enter the path to the .txt file containing the ftp download paths.

~~~~~

Figure 3. 5 *Meteorological Data download script*

The RINEX meteorological files were first uncompressed using windows winRAR app to get its uncompressed file (xxxxddd.yy) so as it can be read by GAMIT.GLOBK software.

3.4 Data processing

The processing of prepared data for this study was mainly based on GPS processing software GAMIT/GLOBK in which the results went through some statistical testing with help of other software including MATLAB and Microsoft office excel. All necessary Data were prepared for processing and arranged in their respective folders for each year (rinex, brdc, gsoln, igs and meteofiles), the data were subjected to GAMIT/GLOBK processing. GAMIT/GLOBK is a comprehensive GPS analysis package developed at MIT, the Harvard Smithsonian Centre for Astrophysics (CfA), Scripps Institution of Oceanography (SIO), and Australian National University for estimating station coordinates and velocities, stochastic or functional representations of post-seismic deformation, atmospheric delays, satellite orbits, and Earth orientation parameters (Herring *et al.*, 2015).

3.4.1 Data processing by gamit

Creating working directory

After preparing all necessary data for processing and arranging them in respective folders for each year (rinex, brdc,gsoln, igs and meteofiles), the data were subjected to GAMIT/GLOBK for processing the data processed include one year then one top directory was setup for year 2015. In the year directory, five directories were set up where the data for processing were

inputted which were rinex, meteofiles, igs, brdc and gsoln. Figure 3.6 shows the Workflow for processing of GNSS Data by using GAMIT/GLOBK.

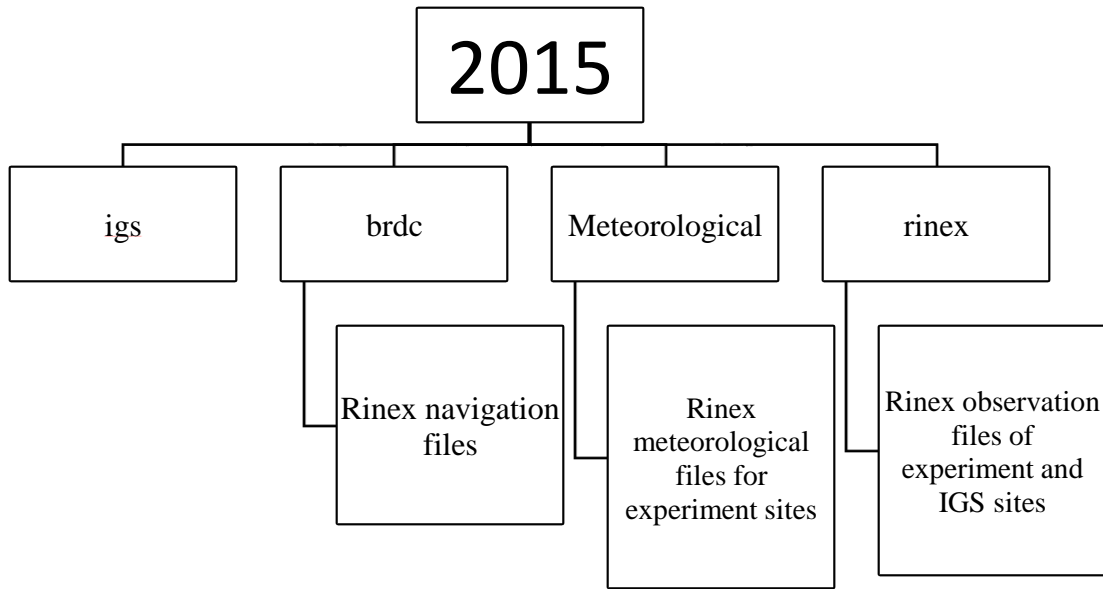


Figure 3. 6 Workflow for processing GNSS Data by using GAMIT Software

3.4.1.1 Creation of tables

Tables were created using `sh_upd -yr [yyyy]` command in respective year directory. The created tables directory contained several files with different station information including `lfile.`, `lfile.old`, `igs14_comb.apr`, `station.info` and other files

3.4.1.2 Updating site information on station.info file

Before updating this info, the rinex files for all sites which were going to be processed were checked and made sure are in the rinex directory. The station information for global sites was refreshed using a specific command. The following command was used to create the station.info `tables>sh_upd_stnfo -l sd` and the output was `station.info.new` then it was renamed as `station.info`. Then the station.info file was updated using experiment and IGS sites from rinex directory using a command `sh_upd_stnfo -files. /rinex/*.15o` which extracts information from RINEX header for each site in respective year.

3.4.1.3 Running sh_gamit to get O-files

With tables already created and updated, the tool `sh_gamit` which comprise of several GAMIT processes to create daily constrained and loosely estimates were run at year level

directory. The `sh_gamit` command was as shown in the figure 3.7 below whereby the name of the experiment site was set as *test*. The command was executed for each day for all sites.

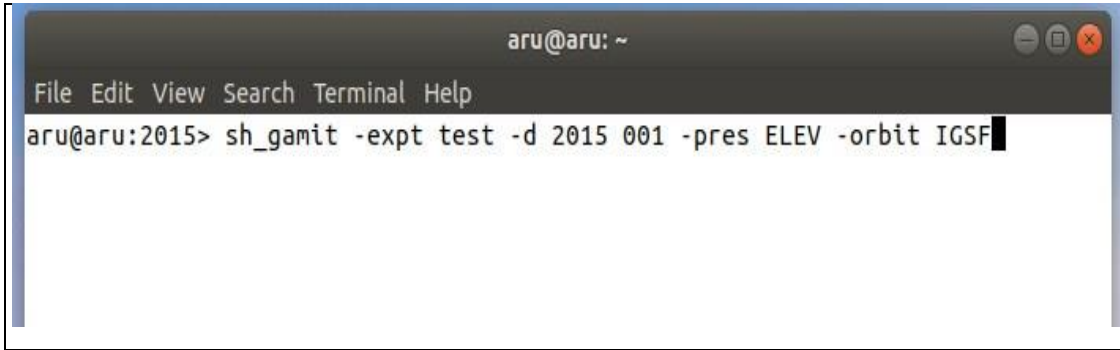


Figure 3. 7 *Sh_gamit command for processing day 001*

The syntax of the command was as follows;

`sh_gamit -expt test -d [yyyy] [ddd] -pres ELEV -orbit IGSF -copt x k p -dopt c ao` in which the experiment name was set as *test* with orbit file used as IGS final orbit. The command executed in each day following the below described steps. The following are the steps which were carried out when `sh_gamit` was running

- i. Assign parameters of program flow, giving precedence first to the command-line arguments, then to the parameters set in process.Defaults and sites. Defaults, and then to default assignments within `sh_gamit` itself.
- ii.Create the day-directory and/or standard directories which do not yet exist
- iii.Link into the day directory the standard tables sing script links. Day and theRINEX files that contain data at 24hrs interval
- iv.Run `makexp` to create the input files for `makex` (scal. `makex`. Batch) and `fixdrv`
- v.Run `sh_check_sess` to make sure that all of the satellites included in the RINEX obs files are present in the nav file and in the g-file (created previously at MIT from an IGS sp3 file)
- vi.Run `sh_make` to create a j-file of satellite clock estimates from the sp3 file.
- vii.Run `makex` to create x-files (observations) and k-files (receiver clock estimates) using phase and pseudorange data from RINEX obs,nav and j-file.
- viii.Run `fixdrv` to create the batch file for GAMIT/GLOBK processing

ix. Execute the batch run to generate a tabular orbital ephemeris (arc), model the phase observations (model), edit the data (autcln), and estimate parameters (solve) and save the cleaning summary.

With this sequence of operation, outputs were produced and the output O-file was of interest for this research. The o-file is an output from solve *run* which contains necessary information which are inputs to utility sh_metutil. It contains the parameters of the piecewise-linear model estimated from the data, which metutil will interpolate to obtain ZTD (Herring *et al.*, 2015).

The script that was used to process all data in sh_gamit for all the RINEX observation files for both experiment and IGS sites is shown in figure 3.5 below whereby it is a sample for day 301 to 367.

```
#!/bin/csh -f
#
set day = 301
while ($day < 367)
echo "starting processing sh_gamit day" $day
sh_gamit -expt test -d 2015 $day -pres ELEV -orbit IGSF -copt x k p -dopts c ao
echo "Completed processing sh_gamit day" $day

@ day = $day + 1
end
```

Figure 3. 8 A sample script showing processing for day 301 to 367

3.4.1.4 Running the utility sh_metutil

After obtaining the O-files as an output from sh_gamit then the next step was running the sh_metutil to obtain the estimated atmospheric values. The o-files were copied into the meteofiles directory which also contained the RINEX met files xxxxxxxx.yym. The utility sh_metutil was then run whereby the inputs were the o-files and RINEX met files and then to obtain the output file which will be in the format of met_[site]. [yyddd].

The scripts induced were of three different parts which covered the whole year of 365 days which were created for the repetition of each process for all days. The prepared scripts

were named as srk1.csh, srk2.csh and srk3 for day 1-9, day 10-99 and day 100-365 respectively. Table 3-9, 3-10 and 3-11 shows the scripts used for the utility sh_metutil

```
#!/bin/csh -f
#
set day = 1
while ("00"$day < 10)
echo "starting processing sh_metutil day" $day
sh_metutil -f otesta."00"$day -m dodm"00"$day"00".15m
echo "Completed processing sh_metutil day" "00"$day

@ day = "00"$day + 1
end
```

Figure 3. 9 *Script showing processing for day 1 to 9 in utility sh_metutil*

```
#!/bin/csh -f
#
set day = 10
while ("0"$day < 100)
echo "starting processing sh_metutil day" $day
sh_metutil -f otesta."0"$day -m dodm"0"$day"0".15m
echo "Completed processing sh_metutil day" "0"$day

@ day = "0"$day + 1
end
```

Figure 3. 10 *Script showing processing for day 10 to 99*

```
#!/bin/csh -f
#
set day = 100
while ($day < 367)
echo "starting processing sh_metutil day" $day
sh_metutil -f otesta.$day -m mtve$day"0".15m
echo "Completed processing sh_metutil day" $day

@ day = $day + 1
end
```

Figure 3. 11 *Script showing processing for day 100 to 366*

The output files contained ZTD, ZHD, ZWD and PW together with their uncertainties. after renaming all outputs from *met_[site]. [yyddd]* to site *met_[site]. [yyddd].csv* to get excel files. The daily ZHD and ZWD were used in analysis for station of different elevation

CHAPTER FOUR

RESULTS AND ANALYSIS

This chapter includes the discussion and analysis of the results obtained from different processes such as ZHD's and ZWD's. By using the GAMIT program, a number of procedures were used to extract important characteristics, such as the Zenith Hydrostatic delay (ZHD), Zenith Wet Delay (ZWD), and Zenith Total Delay (ZTD). The objective was to compare these values at different elevations and determine the points that are most affected by these delays. By evaluating the ZHD, ZWD, and ZTD values across different elevation ranges. The analysis considered the variations in these delays among the different points, with specific attention given to the points experiencing the greatest influence from these atmospheric effects.

These results provide valuable information on the variability and impact of ZHD, ZWD, and ZTD with respect to elevation. Understanding the degree of influence of these delays at different elevations is essential for accurate positioning and atmospheric correction applications.

4.1 3D positioning

RINEX files from three distinct points were collected, each characterized by a different elevation. These files were processed using the GAMIT software, which employs precise point positioning techniques, precise orbit and clock corrections, atmospheric modelling, and ambiguity resolution. The resulted position from GAMIT provides X, Y, and Z coordinates of ARSH, DODM and MTVE stations. These coordinates represent the precise location of point in the geocentric cartesian coordinate system as shown on table 4-1.

Table 4- 1 *3D position of stations*

STATION	Longitude °	Latitude °	Height (m)
ARSH	36.698°	-3.387°	1345.161
DODM	35.748°	-6.187°	1122.595
MTVE	40.166°	-10.26°	-11.414

The solutions were then analysed to evaluate the variations caused by differences in elevation. The primary objective was to analyse the differences in elevation results between points at varying positions, particularly assessing the impact of elevation differences greater than 100 meters.

4.2 Zenith Hydrostatic Delay ZHD

Zenith Hydrostatic Delay or Dry Delay uses estimated or measured ground meteorological data. By examining ZHD across different elevation points, higher elevations exhibit lower ZHD values due to the reduced atmospheric column thickness, while lower elevations tend to have higher ZHD values due to the thicker atmospheric column. Table 4-2 shows the mean ZHD values of the stations also the highest ZHD value and lowest ZHD value over the period of one year (2015). Also, ZHD values exhibit seasonal trends due to changes in atmospheric conditions, such as air pressure, temperature, and humidity.

Table 4- 2 *Mean ZHD values of stations*

STATION	ELEVATION (m)	Highest ZHD value (mm of water vapour)	Lowest ZHD value (mm of water vapour)	Mean ZHD value (mm of water vapour)
ARSH	1345.161	1994.17	1964.47	1980.84
DODM	1122.595	2045.36	2014.29	2030.97
MTVE	-11.414	2320.58	2293.17	2306.12

From table 4-2, higher elevation station ARSH (1345.161 m) and DODM (1122.595m) exhibit lower ZHD's 1980.84mm of water vapour and 2030.97mm of water vapour respectively compared to lower elevation station MTVE (-11.414m) which exhibit higher ZHD of 2306.12mm of water vapour.

4.2.1 Graph of ZHD against elevation

As elevation increases, the graph shows a decrease in ZHD or dry delay. This decrease is attributed to surface pressure measurements, which vary with elevation. Consequently, the variation in pressure results in variations in ZHD. High elevations experience less delay compared to low elevations, where delays are more significant. This discrepancy is due to the

differences in surface pressure as elevation changes. Thus, GNSS signals at higher elevations are less affected by delays compared to lower elevation points. Figure 4.1, 4.2 and 4.3 shows the graph trends of ZHD from Dec 2014 to Jan 2016 for ARSH, DODM and MTVE stations respectively. While figure 4.4 shows the difference ZHD trends for points of different elevation.

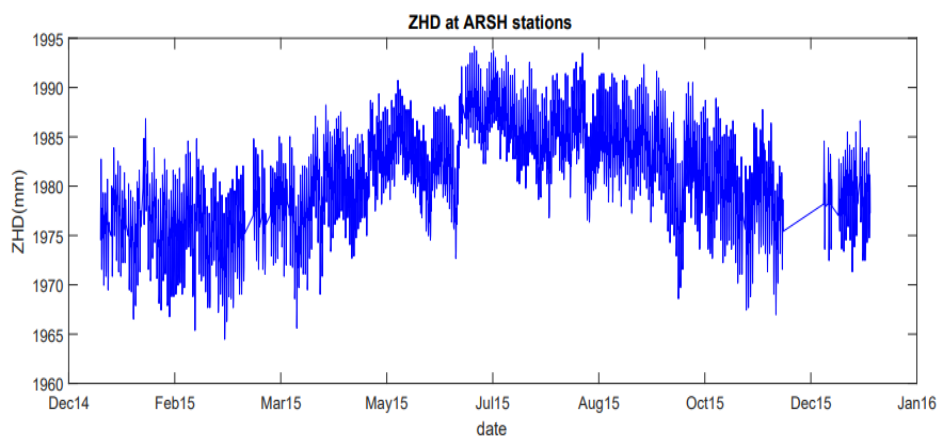


Figure 4.1 Graph showing ZHD trend at ARSH station

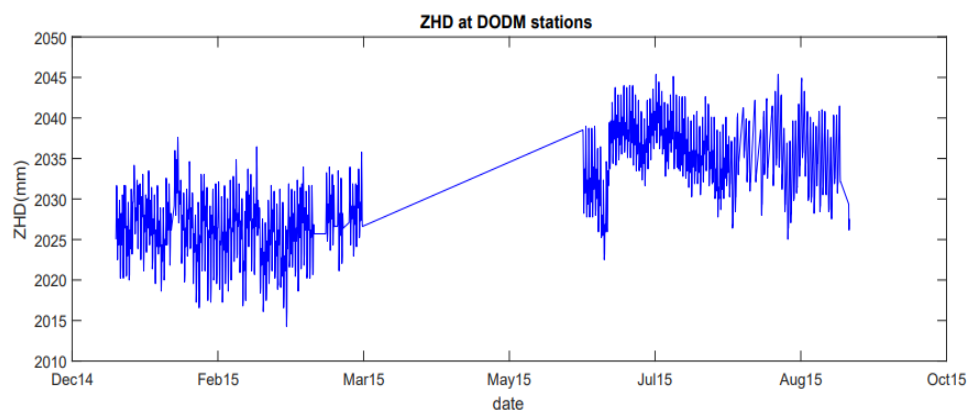


Figure 4.2 Graph showing ZHD trend at DODM station

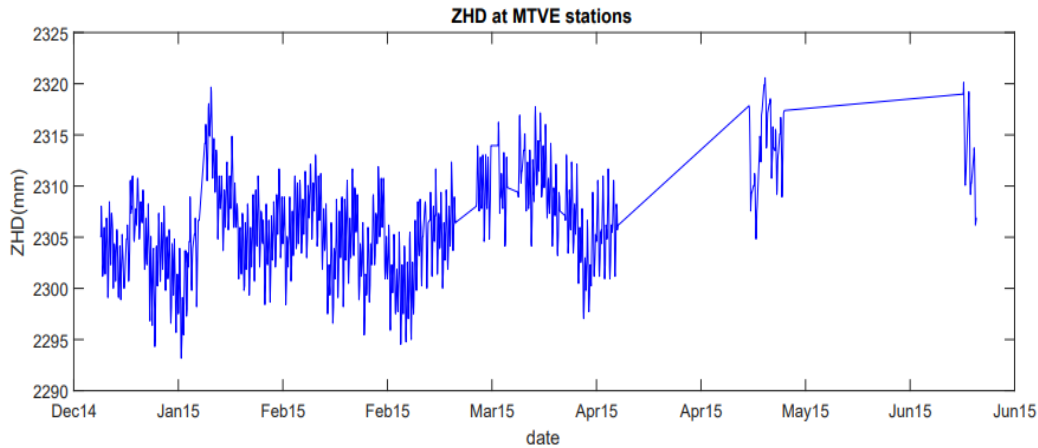


Figure 4.3 Graph showing ZHD trend at MTVE station

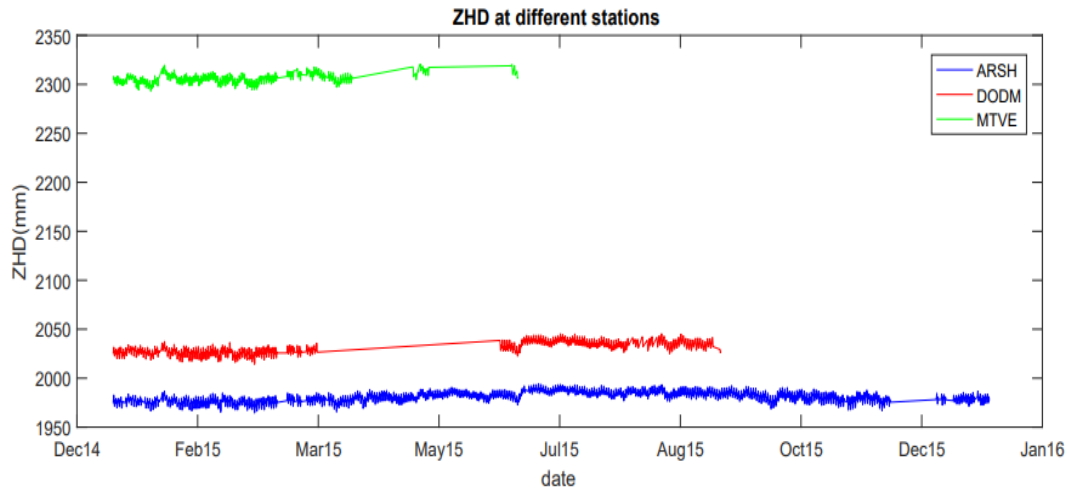


Figure 4.4 Graph showing ZHD for points of different elevation

4.3 Zenith Wet Delay

Zenith Wet Delay depends on atmospheric water vapour pressure and it does not depend on surface measurement of meteorological data. As the elevation increases, the zenith wet delay generally tends to decrease. Higher elevation points are generally less affected by atmospheric moisture delays. Table 4-3 shows the mean ZWD values of the stations also the highest ZWD value and lowest ZWD value over the period of one year (2015).

Table 4- 3 *Mean ZWD values for points of different elevation*

STATION	Elevation (m)	Highest ZWD value (mm of water vapour)	Lowest ZWD value (mm of water vapour)	Mean ZWD value (mm of water vapour)
ARSH	1345.161	261.39	64.67	163.62
DODM	1122.595	269.99	56.69	162.10
MTVE	-11.414	402.55	112.58	309.55

From the table 4-3, below higher elevation station ARSH (1345.161 m) and DODM (1122.595m) exhibit lower ZWD's 163.62mm of water vapour and 162.10mm of water vapour respectively compared to lower elevation station MTVE (-11.414m) which exhibit higher ZWD of 309.55mm of water vapour. Also, Regions with consistent dry weather or arid climates tend to exhibit lower zenith wet delay values, regardless of elevation for example at DODM station which located at Dodoma Region which exhibit the lowest ZWD value despite its not the highest elevation point.

The analysis demonstrates that zenith wet delay exhibits a decreasing trend with increasing elevation, indicating lower moisture content and reduced atmospheric delays. This information can contribute to more accurate GNSS measurements and enhance various applications relying on satellite positioning systems.

4.3.1 Graphs of ZWD

As shown on the graphs (Figure 4.5, 4.6, 4.7 and 4.8) below ZWD changes as the elevation of the points varies. Generally, as the elevation increases, the ZWD tends to decrease. This relationship suggests that higher elevation points experience lower atmospheric moisture content, resulting in reduced delays caused by water vapour. This trend suggests that higher elevation points experience less atmospheric moisture delay compared to lower elevation points. The zenith wet delay is influenced by the amount of moisture in the atmosphere. Higher elevations typically exhibit drier atmospheric conditions, resulting in lower zenith wet delay values. In contrast, lower elevation areas may have more moisture content, leading to higher zenith wet delay values. Figure 4.5, 4.6 and 4.7 shows the graph

trends of ZWD from Dec 2014 to Jan 2016 for ARSH, DODM and MTVE stations respectively. While figure 4.8 shows the difference ZWD trends for points of different elevation.

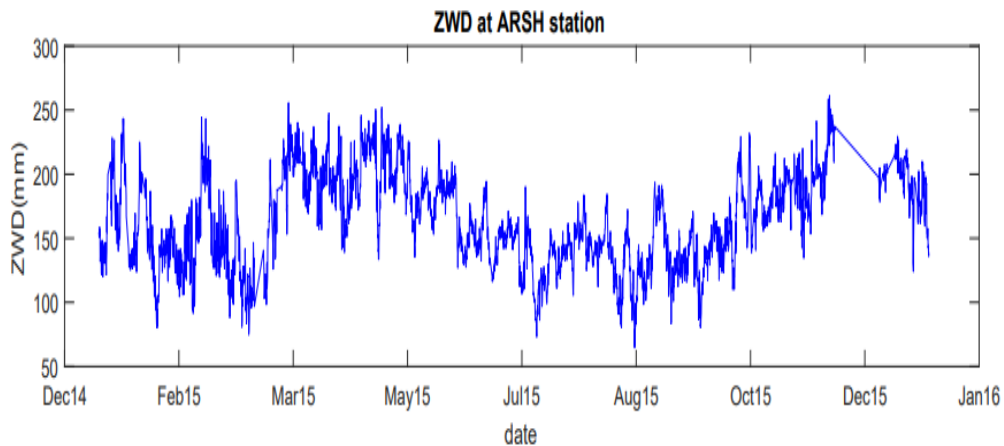


Figure 4.5 Graph showing ZWD trend at ARSH station

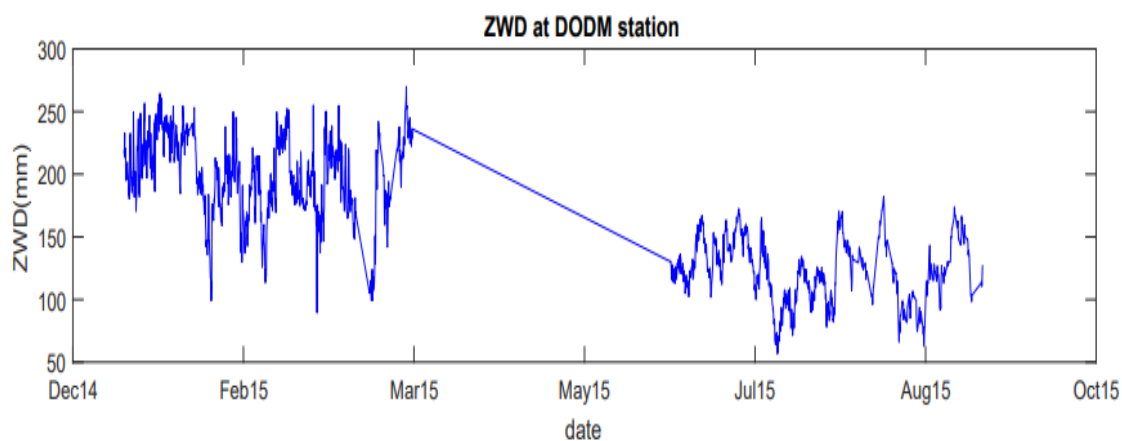


Figure 4.6 Graph showing ZWD trend at DODM station

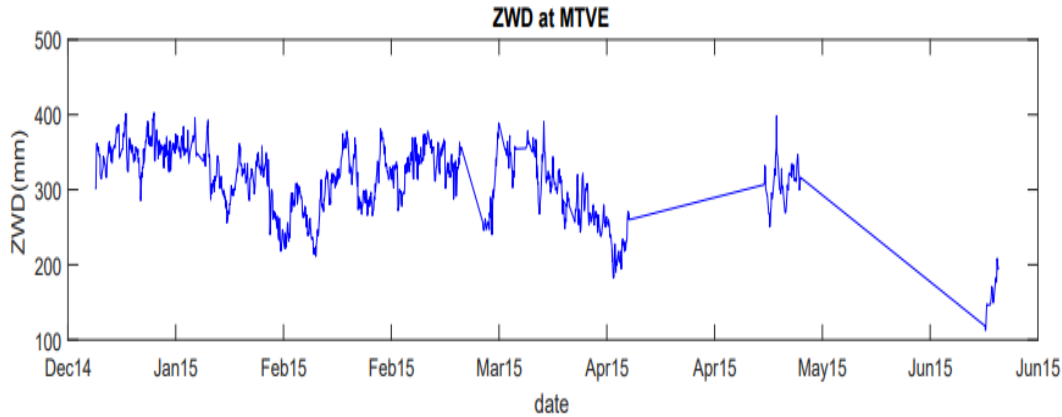


Figure 4.7 Graph showing ZWD trend at MTVE station

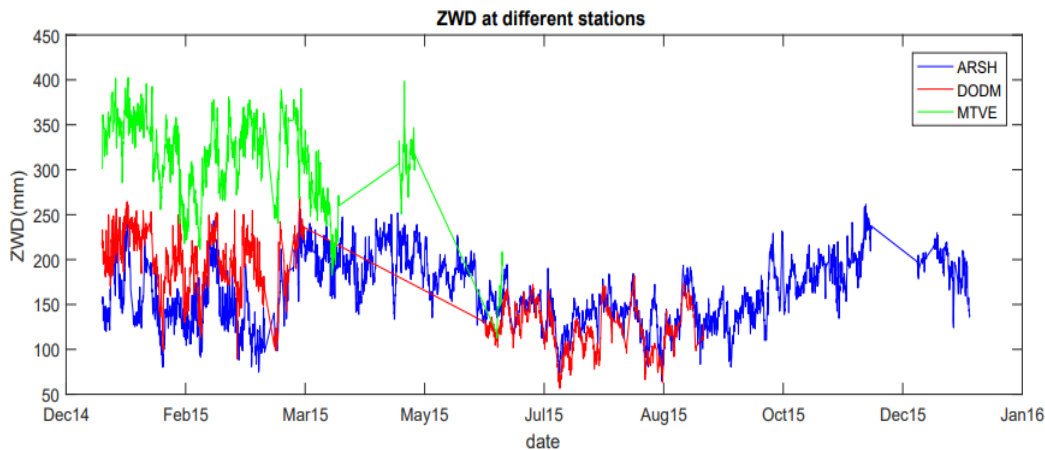


Figure 4.8 Graph showing ZWD trends for points of different elevation

Also, the downward trend in ZWD with increasing elevation implies that regions at higher elevations typically have drier atmospheric conditions compared to lower elevations. This can be attributed to factors such as reduced proximity to moisture sources like bodies of water or changes in air mass characteristics with elevation. Appendix I and II shows graphs of ZWD's for points of different elevation.

4.4 Zenith Total Delay

As from equation 2.8 ZTD is obtained by taking summation of ZHD and ZWD. Table 4-4 shows the Mean ZTD from the summation of Mean ZHD and ZWD for ARSH, DODM and MTVE with their elevations.

Table 4-4 *Mean ZTD values of stations*

STATION	ELEVATION	Mean ZHD (mm of water vapour)	Mean ZWD (mm of water vapour)	Mean ZTD (mm of water vapour)
ARSH	1345.161	1980.84	163.62	2144.46
DODM	1122.595	2030.97	162.10	2193.07
MTVE	-11.414	2306.12	309.55	2615.67

ZTD values exhibit a relationship with elevation, where higher elevation points tend to have lower ZTD values compared to lower elevation points. This relationship can be attributed to variations in atmospheric moisture content and mass with changes in elevation. ZTD values at different elevations reflect the moisture content in the atmosphere. Generally, higher elevation points experience drier atmospheric conditions, resulting in lower ZTD values. In contrast, lower elevation areas may have higher moisture content, leading to higher ZTD values. Also, ZTD is influenced by the atmospheric mass, which is related to the weight of the air column above a specific point. As elevation increases, the atmospheric mass decreases, resulting in a reduction in ZTD values. This is because there is less air mass to cause delays in the signal propagation.

4.4.1 Graph of ZTD

The graph below shows that the ZTD it varies with height in which as height increases the zenith total delay decrease. This suggests that higher elevation locations experience less delay than lower elevation ones, which display more delay. The variation in ZTD with height is influenced by atmospheric factors such as moisture content and atmospheric mass. Generally, higher elevation points tend to have lower moisture content and reduced atmospheric mass, resulting in decreased ZTD values. Figure 4.9 shows the ZTD trends for points of different elevation from Dec 2014 to Jan 2016 also Figure 4.10 shows the uncertainty or variability associated with data points.

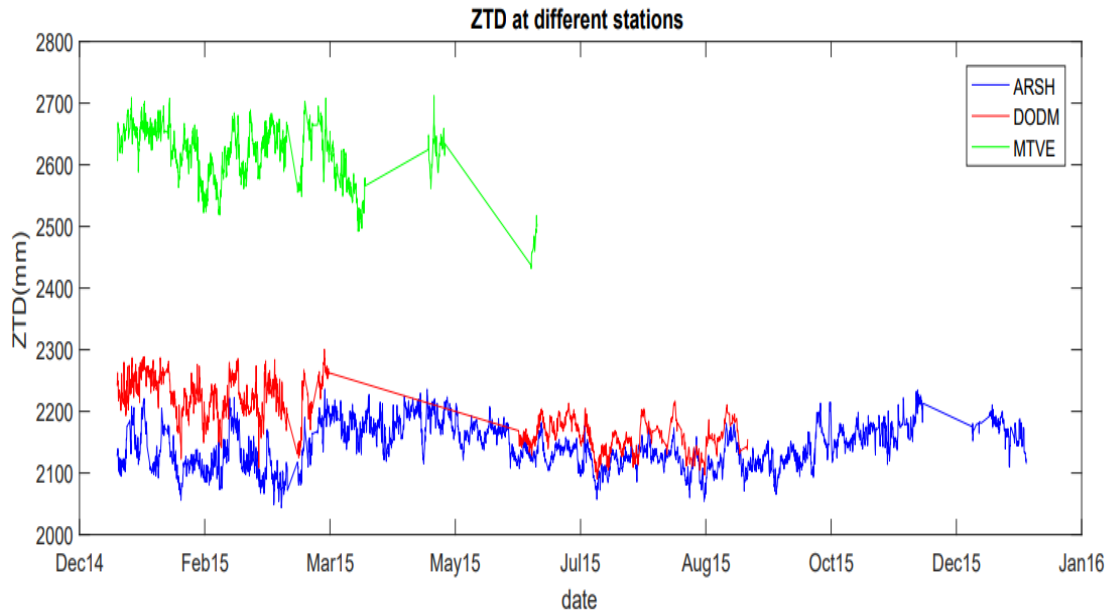


Figure 4.9 Graph showing ZTD trend for points of different elevation

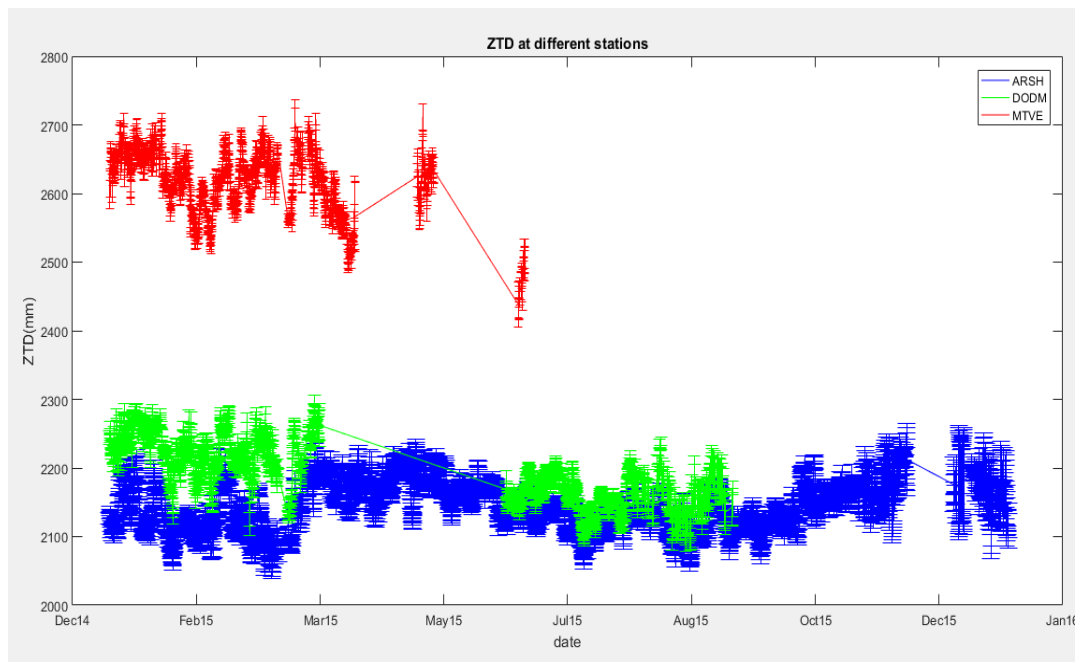


Figure 4. 10 Graph shows error bar for ZTD values for points of different station

The decreasing ZTD values as height increases imply that points at higher elevations experience less atmospheric delay in GNSS signal propagation. This reduction in delay

contributes to improved accuracy in positioning and timing applications for these points. While the graph indicates a general trend, it's important to consider that geographic factors and local conditions can influence ZTD values. Factors such as proximity to large water bodies, topography, and vegetation cover can introduce variability even among points at similar elevations. And from figure 4.10 the graph shows the uncertainty or variability associated with data points and the values are within the limited accuracy.

CHAPTER FIVE

CONCLUSION AND RECOMMENDATION

5.1 Conclusion

From the finding of this research a successfully determination of Zenith Tropospheric Delay (ZTD), Zenith Hydrostatic Delay (ZHD), and Zenith Wet Delay (ZWD), which affects GNSS signals from the satellite to receiver of different points at different elevation.

From these results and analysis done on chapter four ZHD varies due to tropospheric thickness variation in different elevation but also differences in surface pressure as elevation changes also cause to variation on ZHD. And for ZWD it varies due to variation of atmospheric moisture delays, as higher elevation points experience lower atmospheric moisture content, resulting in reduced delays caused by water vapour. But also, Higher elevations typically exhibit drier atmospheric conditions, resulting in lower zenith wet delay values. And lower elevation areas may have more moisture content, leading to higher zenith wet delay values.

Also, Regions with consistent dry weather or arid climates tend to exhibit lower zenith wet delay values, regardless of elevation. And ZTD values decreases as height increases imply that points at higher elevations experience less atmospheric delay in GNSS signal propagation. For example, ARSH (1345.161m) have more less delay of 2144.46mm compared to the other low elevation point MTVE (-11.414m) which have large delay of 2615.67mm the variation of atmospheric temperature and pressure with height which contributed to delay of GNSS signals from the satellite to receiver. In which temperature varies at lapse rate (6.5°C per 1000m) so that the GSS signals travel a short distance in high elevation (less delay) compared to points with low elevation.

5.2 Recommendation

From the finding of this study the following recommendation are given;

- I. Further research can explore the specific relationships between ZTD, elevation, and other atmospheric parameters. Investigating long-term trends, studying different geographical regions, and considering the influence of local weather patterns can provide deeper insights into the elevation-dependent behaviour of ZTD.
- II. Furthermore, it would be beneficial to conduct additional research focusing on stations located at different positions but with similar elevations investigate the effects that contribute to variations in delay, apart from elevation alone. This exploration would allow us to identify and understand other factors that may influence the increase or decrease in delay. Analysing stations with comparable elevations but different positions can provide valuable insights into the complex relationship between delay and various environmental factors.

REFERENCES

- Acheampong, A. (2008). *Developing a Differential GPS (DGPS) Services in Ghana*. Kwame Nkrumah University of Science and Technology.
- Acheampong, A. A. (2015). *Retrieval of Integrated Water Vapour from GNSS Signals for Numerical Weather Predictions (Issue August)*. Kwame Nkrumah University of Science and Technology.
- Awange, L. J. (2012). *Environmental Monitoring Using GNSS*. Springer.
- Bevis, M. H. (1994). *GPS Meteorology : Mapping Zenith Wet Delays onto Precipitable Water*.
- Combrinck, L. (2015, november). Performance Evaluation of Blind Tropospheric Delay correction Models over.
- Davis, J. L., Herrinch, T. A., Shapiro, I. I., Rodgers, A. E., & Elgered, G. (1985). *Geodesy by radio interferometry: Effects of atmospheric modeling errors on estimates of baseline length*. *Radio Science*, 20(6).
- Diggelen, F. V. (2009). *A GPS, Assisted GPS, GNSS and SBAS*. Artech house.
- Ghoddousi-fard, R., & Dare, P. (2006). *Online GPS processing services : an initial study*.
- Herring, T. A., King, R. W., Floyd, M. A., McCluskey, S. C., & Sciences, P. (2015). *Gamit reference manual analysis at MIT*.
- Hofmann-Wellenhof, B., Lichtenegger, H., & Wasle. (2020). *GNSS – Global Navigation Satellite Systems GPS, GLONASS, Galileo, and more*. Springer Wien New York.
- Kleijer, F. (2004). *Troposphere Modeling and Filtering for Precise GPS Leveling*. Netherlands: Technische Universiteit Delft.
- Leandro. (2006). *UNB Neural Atmosphere Models: Development and Performance*. California, USA: Monterey.
- Lechner, W., & Baumann, S. (2000). *Global navigation satellite systems*.
- Misra, P. &. (2011). *Global Positioning System : Signals , Measurements , and Performance*. Ganga-Jamuna Press.

- Misra, P., & Enge, P. (2011). *Global Positioning System : Signals , Measurements , and Performance*. Ganga-Jamuna Press.
- Mohindre, S. G., Angus, P. A., & Chris, G. B. (2013). *Global Navigation Sattelites System, Inertial Navigation and Intergration 3rd edition*. Canada: JOHN WILEY & SONS,INC.
- Niell, A. E. (1996). *Global mapping functions for the atmosphere delay at radio wavelengths*.
- Njau, A. (2021). *Assesment Of 3D Position Accuracy Of GNSS Receiver Due To Tropospheric Variation At Different Elevation*. Dar es salaam: Ardhi University.
- Pratap. (2006). *Global Positioning System*. United States of America: Ganga Jumana Press.
- Rabbany, A. E. (2002). *Introduction to Global Position System*. Artech house.
- Ramos-Bosch, P. (2019). *ESA GNSS Education: GNSS-Lab tool Software User Manual*.
- Reguzzoni, I. (2013). *Gps Tropospheric delay for meteorological application*.
- ROB-Editors. (2016). *How GNSS Works*.
- Seeber, G. (2003). *Satellite Geodesy de Gruyter (second)*.
- Selbesoglu, M. O. (2019, september 3). Spatial Interpolation of GNSS Troposphere Wet Delay by a Newly Designed Artificial Neural Network Model.
- Selbesoglu, M. O. (2019). *Spatial Interpolation of GNSS Troposphere Wet Delay by a Newly Designed Artificial Neural Network Model*.
- Shrestha, S. M. (2013). *Investigation into the Estimation of tropospheric delay Using Different Data in Iran*.
- Sickle, J. V. (2008). *Gps for Land Surveyors*. Tylor&Francis Group.
- Solheim, S. &. (n.d.). *Propagation delays induced in GPS signals by dry air , water vapor , hydrometeors , and other particulates Propagation delays induced in GPS signals by dry air , water vapor , hydrometeors , and other particulates. January*.
- Subirana, S. J., Zornoza, J. J., & Hernánd, M. (May 2013). *GNSS DATA PROCESSING*. Netherlands: ESA Communications.

Subriana, S. J., Hernandez-parajes, M., & Zomoza, J. J. (2014). *GNSS signal*.

USACE-Editors. (2003). *NAVSTAR Global Positioning System Surveying*.

APPENDICES